

On the origins of hierarchy in complex networks

Bernat Corominas-Murtra^{a,b,c}, Joaquín Goñi^d, Ricard V. Solé^{a,b,e,1}, and Carlos Rodríguez-Caso^{a,b,1}

^aInstitució Catalana per a la Recerca i Estudis Avançats–Complex Systems Laboratory, Universitat Pompeu Fabra, 08003 Barcelona, Spain; ^bInstitut de Biologia Evolutiva (Consejo Superior de Investigaciones Científicas–Universitat Pompeu Fabra), 08003 Barcelona, Spain; ^cSection for Science of Complex Systems, Medical University of Vienna, 1090 Vienna, Austria; ^dDepartment of Psychological and Brain Sciences, Indiana University, Bloomington, IN 47405; and ^eSanta Fe Institute, Santa Fe, NM 87501

Edited* by Ignacio Rodriguez-Iturbe, Princeton University, Princeton, NJ, and approved June 24, 2013 (received for review January 17, 2013)

Hierarchy seems to pervade complexity in both living and artificial systems. Despite its relevance, no general theory that captures all features of hierarchy and its origins has been proposed yet. Here we present a formal approach resulting from the convergence of theoretical morphology and network theory that allows constructing a 3D morphospace of hierarchies and hence comparing the hierarchical organization of ecological, cellular, technological, and social networks. Embedded within large voids in the morphospace of all possible hierarchies, four major groups are identified. Two of them match the expected from random networks with similar connectivity, thus suggesting that nonadaptive factors are at work. Ecological and gene networks define the other two, indicating that their topological order is the result of functional constraints. These results are consistent with an exploration of the morphospace, using *in silico* evolved networks.

modularity | evolution

Fifty years ago (1), Herbert Simon defined complex systems as nested hierarchical networks of components organized as interconnected modules. Hierarchy seems a pervasive feature of the organization of natural and artificial systems (2, 3). The examples span from social interactions (4, 5), urban growth (6, 7), and allometric scaling (8) to cell function (9–13), development (14), ecosystem flows (15, 16), river networks (17), brain organization (18), and macroevolution (19, 20). It also seems to pervade a coherent form of organization that allows reducing the costs associated to reliable information transmission (21) and to support efficient genetic and metabolic control in cellular networks (22). However, hierarchy is a polysemous word, involving order, levels, inclusion, or control as possible descriptors (23), none of which captures either its complexity or the problem of its measure and origins. Although previous work using complex networks theory has quantitatively tackled the problem (4, 24–34), some questions remain: Is hierarchy a widespread feature of complex systems organization? What types of hierarchies do exist? Are hierarchies the result of selection pressures or, conversely, do they arise as a by-product of structural constraints?

A well-established concept where such questions are addressed involves the use of a morphospace (35–40), namely a phenotype space where a small set of quantitative traits can be defined as the axes. Here we take a step in this direction by combining morphospace and network theories, taking the intuitive idea of hierarchy as the starting point: a pattern of relations where there is no ambiguity in who controls whom with a pyramidal structure in which the few control the many. Formally, the picture of hierarchy matches a tree of relations (41), ideally represented by a directed graph. As shown in Fig. 1 A–D, the elements of the system are represented by nodes connected by arrows establishing the map of relations of who affects whom. Accordingly, a measure of hierarchy should account for the deviations from this ideal tree picture. Such deviations occur because (a) several elements are on the top, (b) downstream elements interact horizontally, or (c) feedback loops are present. As shown in Fig. 1A, the tree-like picture matches the concept of genealogies, taxonomies, armies, and corporations. Conversely, drainage networks

in river basins (17) would define a reverse antihierarchical situation, as depicted in Fig. 1B. In this structure, multiple elements on the top merge downstream like an inverted tree. In between them, we can place a more or less symmetric web (Fig. 1C), somewhat combining both tendencies. However, in general, neither biological nor technological webs match the feed-forward pattern. In most real systems, signal integration requires gathering inputs from different sources, whereas robust processing and control require crosstalk and feedbacks, as represented by Fig. 1D, which are often organized in a modular fashion (42).

A unified picture of hierarchy should not only provide a formal definition but also help in understanding the forces that shape it. To naturally incorporate both components of Simon's view, namely causal downstream relations plus modules, a network formalism is required. Here we provide the formalization and quantitative characterization of the morphospace of the possible hierarchies. Its characterization is performed by theoretical and numerical analysis of random null models. The study of a large number of real networks and its comparison with model systems provide some unexpected answers to the previous questions. The study is completed with an exploration of the morphospace accessibility, using an evolutionary-driven search algorithm. Technical aspects of this work following the main text's organization are in *SI Appendix*.

The Coordinates of Hierarchy

Because hierarchy is about relations, our approach formalizes the interaction between the system's elements by means of a directed graph $\mathcal{G}(V, E)$ (43), where $v_i \in V$ ($i = 1, \dots, n$) is a node and $\langle v_i, v_j \rangle \in E$ is an arrow going from v_i to v_j (*SI Appendix*). This graph is transformed into the key object for our methodology: the so-called node-weighted condensed graph, $\mathcal{G}_C(V_C, E_C)$. As Fig. 1 D and H shows, \mathcal{G}_C is a feedforward structure where cyclic modules of \mathcal{G} [the so-called strongly connected components (SCCs) $\{S_1, \dots, S_\ell\}$] are represented by individual nodes (thereby obtaining the condensed graph) (43). Such SCC method detection has been shown to be a powerful approach for subsystem identification (13, 44, 45), unraveling the presence of nested organizations. In a given \mathcal{G}_C , every node has a weight α_i that indicates the number of elements from \mathcal{G} it includes (details in *SI Appendix*). By using \mathcal{G}_C , we make explicit the inclusion of both causal links and irreducible modules.

Our space of hierarchies is a metric space Ω , defined from three coordinates: treeness (T), feedforwardness (F), and orderability (O), which properly quantify graph hierarchy.

Author contributions: B.C.-M., J.G., R.V.S., and C.R.-C. designed research; B.C.-M., J.G., and C.R.-C. performed research; B.C.-M., J.G., and C.R.-C. contributed new reagents/analytic tools; B.C.-M., J.G., R.V.S., and C.R.-C. analyzed data; B.C.-M., R.V.S., and C.R.-C. wrote the paper; and J.G. performed programming and computational analysis.

The authors declare no conflict of interest.

*This Direct Submission article had a prearranged editor.

¹To whom correspondence may be addressed. E-mail: carlos.rodriguez@upf.edu or ricard.sole@upf.edu.

This article contains supporting information online at www.pnas.org/lookup/suppl/doi:10.1073/pnas.1300832110/-DCSupplemental.

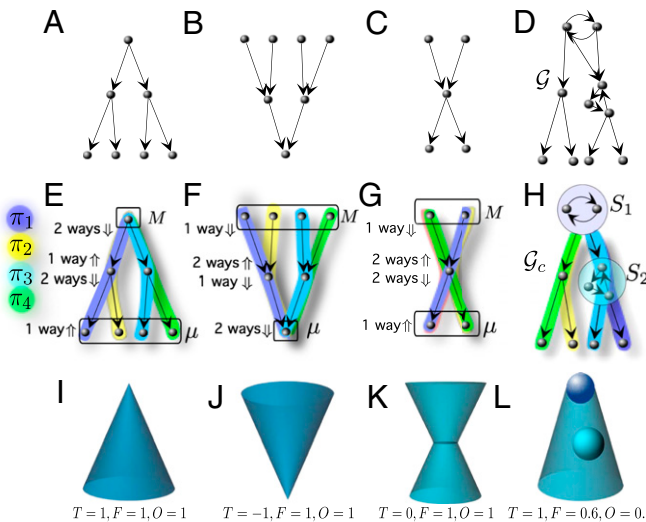


Fig. 1. Different network organizations following the idea of hierarchy. (*A*) The ideal hierarchy seen as a tree-like feedforward graph. (*B*) An inverted tree matching the antihierarchical. (*C* and *D*) A nonhierarchical fan-like feedforward graph (*C*) and a graph \mathcal{G} displaying cycles (*D*). In *E* and *F*, all of them present four pathways ($\pi_1, \pi_2, \pi_3, \pi_4$) from maximals M (top nodes) to minimals μ (bottom nodes). In *E*, downstream diversity of paths is $H_f(\mathcal{G}) = \log 4$ without uncertainty when reversing them; i.e., $H_b(\mathcal{G}) = 0$. *F* depicts the opposite behavior: $H_f(\mathcal{G}) = 0$ and $H_b(\mathcal{G}) = \log 4$. (*G*) A nonhierarchical feedforward structure with the same forward and backward uncertainties, where $H_f(\mathcal{G}) = H_b(\mathcal{G}) = \log 2$. The node-weighted condensed graph, \mathcal{G}_c , was computed by SCC detection labeled by every S_i . (*H*) For S_1 and S_2 , the node weights are $\alpha_1 = 2$ and $\alpha_2 = 3$, respectively. (*I–L*) With a representative icon involving cones and balls, charts show representative TFO values for (*A–D*) graphs.

Treeness. Treeness (T , being T in the range $-1 \leq T \leq 1$) weights how pyramidal is the structure and how unambiguous is its chain of command. This measure covers the range from hierarchical ($T > 0$, Fig. 1*A*) to antihierarchical ($T < 0$, Fig. 1*B*) graphs, including those structures that do not exhibit any pyramidal behavior ($T = 0$, Fig. 1*C*). As illustrated in Fig. 1*E–G*, these graphs are characterized by taking the structure as a road map where we compare the diversity of choices we can make going top-down, i.e., following the arrows of the structure, vs. the uncertainty generated when reverting the paths going bottom-up. Such diversity is properly quantified using forward (H_f) and backward (H_b) entropies, respectively. Entropies are computed over directed acyclic graphs (28, 46). Although *SI Appendix* presents a rigorous description of these concepts, they are briefly presented departing from the node-weighted condensed graph $\mathcal{G}_c(V_c, E_c)$ shown in Fig. 1*H*. Note that a directed acyclic graph is naturally a node-weighted graph and hence ensures $\mathcal{G} = \mathcal{G}_c$. From the graph \mathcal{G}_c , we define two sets, namely M and μ : the first, composed of nodes with $k_{in} = 0$, i.e., the set of maximal nodes, and the second, the set of nodes with $k_{out} = 0$, referred to as the set of minimal nodes. Now, let $\Pi_{M\mu}$ be the set of all paths starting in some maximal node. Because \mathcal{G}_c is a graph without cycles, this set contains a finite number of elements π_1, \dots, π_N . If $v_i \in M$, the information required to follow a given path starting from v_i and ending at some node in μ , $h_f(v_i)$ will be given by the following path entropy,

$$h_f(v_i) = - \sum_{\pi_k \in \Pi_{M\mu}} \mathbb{P}(\pi_k | v_i) \log \mathbb{P}(\pi_k | v_i),$$

where $\mathbb{P}(\pi_k | v_i)$ is the probability that the path π_k is followed, starting from node $v_i \in M$. Averaging this entropy over all paths from M to μ gives the average minimum information required to follow a path starting from some node in M . This reads

$H_f(\mathcal{G}_c) = \frac{1}{|M|} \sum_{v_i \in M} h_f(v_i)$, which is the general expression of the forward entropy of \mathcal{G}_c . In a similar way but in the bottom-up direction, a backward entropy $H_b(\mathcal{G}_c)$ of \mathcal{G}_c can be obtained. $H_b(\mathcal{G}_c)$ represents the average amount of information required to reverse a path $\pi_j \in \Pi_{M\mu}$. A detailed derivation of both $H_f(\mathcal{G}_c)$ and $H_b(\mathcal{G}_c)$ is given in *SI Appendix*. Roughly speaking, a system such that $H_f(\mathcal{G}_c) > H_b(\mathcal{G}_c)$ is considered as hierarchical.

Our measure of treeness is now obtained from the normalized difference (28) of the two entropies:

$$f(\mathcal{G}) = \frac{H_f(\mathcal{G}_c) - H_b(\mathcal{G}_c)}{\max\{H_f(\mathcal{G}_c), H_b(\mathcal{G}_c)\}}$$

[consistently, we have $f(\mathcal{G}) \equiv 0$ if $H_f(\mathcal{G}_c) = H_b(\mathcal{G}_c) = 0$, which takes place when \mathcal{G}_c is a linear chain]. The final value $T(\mathcal{G})$ is computed as follows: First, let $\mathcal{W}(\mathcal{G})$ be the set containing \mathcal{G}_c and all subgraphs of \mathcal{G}_c that can be obtained by means of the application of a leaf removal algorithm (either top-down or bottom-up; details in *SI Appendix*). Then, $T(\mathcal{G})$ is obtained by averaging f along all of the members of $\mathcal{W}(\mathcal{G})$:

$$T(\mathcal{G}) = \langle f \rangle_{\mathcal{W}(\mathcal{G})}. \quad [1]$$

In addition, $T(\mathcal{G}) \equiv 0$ if \mathcal{G}_c has no links—which can happen, e.g., if \mathcal{G} is totally cyclic. $T(\mathcal{G})$ has been shown to be a very good indicator of the deviations of a given acyclic graph from the ideal hierarchical, tree-like picture (28).

Feedforwardness. In the \mathcal{G}_c , because the elements within a SCC cannot be intrinsically ordered, SCCs constitute nonorderable modules within the feedforward structure. As Fig. 1*H* shows, SCCs represent a violation of the downstream order. Here, the size of the SCCs and also their position in the feedforward structure are key elements for the quantification of the impact of cyclic modules in the feedforward structure, because the higher the SCC position, the larger the number of its downstream dependencies. According to this, we define feedforwardness (F , being $0 \leq F \leq 1$) as a measure that weights the impact of cyclic modules on the feedforward structure, where cyclic modules closer to the top of \mathcal{G} introduce a larger penalty on hierarchical order than those placed at the bottom. For every path π_k starting from the top of \mathcal{G}_c we compute the fraction of the nodes that it contains against the actual nodes of \mathcal{G} it represents. Formally, if $v(\pi_k)$ is the set of nodes participating in the path π_k ,

$$F(\pi_k) = \frac{|v(\pi_k)|}{\sum_{v_i \in v(\pi_k)} \alpha_i},$$

where, as illustrated in Fig. 1, α_i is the weight of node v_i in the node-weighted condensed graph. To obtain a statistical estimator of the impact of the location of cyclic modules within the causal flow described by the network, we first have to define the set Π_M , which is the set containing all possible paths starting from the set of maximal nodes, M , and ending in any other node of \mathcal{G}_c . Now, $F(\mathcal{G})$ is, thus, simply the average of $F(\pi_k)$ over all elements of Π_M ; i.e.,

$$F(\mathcal{G}) = \langle F \rangle_{\Pi_M}. \quad [2]$$

Orderability. As hierarchy is grounded on the concept of order, we need a descriptor that accounts for how orderable is the graph under study. Ranging from a fully cyclic graph to a feed-forward structure, orderability (O) lies in the range $0 \leq O \leq 1$ and it is defined as the fraction of the nodes of the graph \mathcal{G} that does not belong to any cycle. These nodes, therefore, make part of the fraction of the network that can be actually ordered. Such

a fraction weights how ordered is the set of nodes within the graph (Fig. 1 *I–L* and *SI Appendix*). Formally, we define $O(\mathcal{G})$ as

$$O(\mathcal{G}) = \frac{|\{v_i \in V_C \cap V\}|}{|V|}. \quad [3]$$

Having exposed the formal description of the different hierarchy indicators, i.e., T , F , and O , we proceed to use them as the axes of our morphospace Ω , where networks can be properly located and compared.

The Definition of the Morphospace Ω

According to our formalism, the hierarchical features of any directed network are given by a point $\mathbf{u}(\mathcal{G})$ in a 3D morphospace Ω , being $\Omega \subset [-1, 1] \times [0, 1] \times [0, 1]$ (Fig. 2*A* and *SI Appendix*, Figs. S13 and S14). The point $\mathbf{u}(\mathcal{G})$ represents the graph \mathcal{G} by three coordinates,

$$\mathbf{u}(\mathcal{G}) = (T(\mathcal{G}), F(\mathcal{G}), O(\mathcal{G})) \in \Omega. \quad [4]$$

Using the schematic representation of graphs outlined in Fig. 1, we define an intuitive icon associated to each kind of graph. As summarized in Fig. 2*A*, the perfect hierarchy is located

at $\mathbf{u}(\mathcal{G}) = (1, 1, 1)$, whereas the completely nonhierarchical system—a totally cyclic network—is located at $\mathbf{u}(\mathcal{G}) = (0, 0, 0)$. As defined, orderability and feedforwardness provide complementary information that defines forbidden regions of the morphospace. Because $F(\mathcal{G}) = 1$ is possible only when $O(\mathcal{G}) = 1$, feedforward networks belong to the $F(\mathcal{G}) = O(\mathcal{G}) = 1$ line. Given $O(\mathcal{G}) = 1$, no other $F(\mathcal{G}) \neq 1$ is allowed. Attending to F and O , we find an interesting region, defined by $O(\mathcal{G}) = 0$ and $F(\mathcal{G}) > 0$. It is worth stressing that, although $O(\mathcal{G})$ and $F(\mathcal{G})$ converge in their upper bound in a single value that defines the region of feedforward networks, they differ when O goes to zero. This is because $F(\mathcal{G})$ deals with the condensed graph while including condensed modules but $O(\mathcal{G})$ is about the nodes outside cycles. This little difference permits a family of rare networks, highlighted in our diagram by means of green icons in Fig. 1*A* (*SI Appendix*, Fig. S13). They are typically formed by chains of small SCCs arranged in a feedforward structure. As is shown below, no such networks are found in nature or technology: They belong to the domain of the possible, but not the actual.

From these two axes accounting for the cyclic nature of networks, the coordinate T provides additional information about the organization of the resulting feedforward structure after network condensation. Attending to the concept of a pyramidal

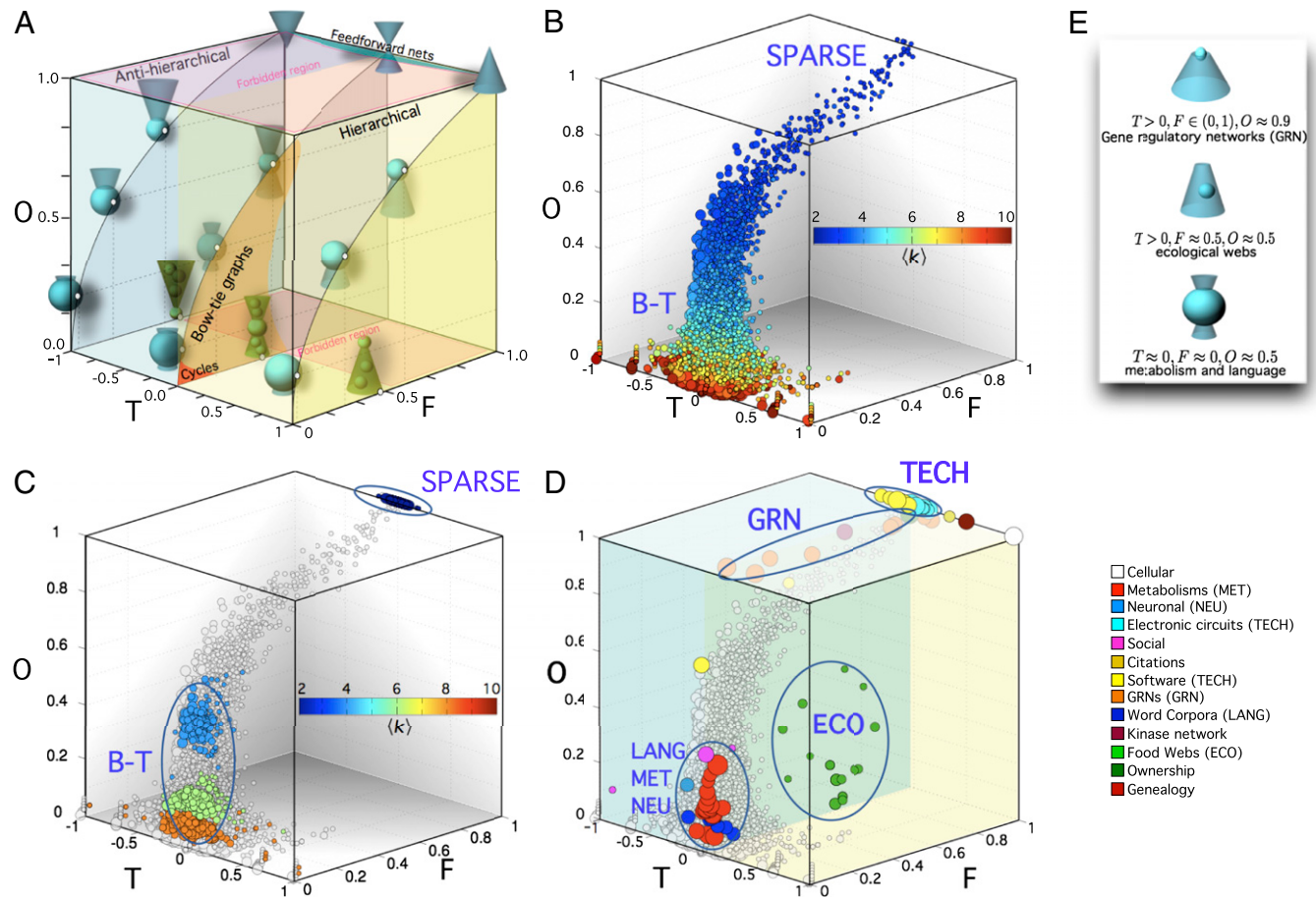


Fig. 2. The morphospace of possible hierarchies Ω . (A) Different morphologies and their respective location within Ω (Fig 1). Green icons represent unlikely configurations (see *SI Appendix* for more information). (B and C) The occupation of Ω by an ensemble of random models. This set includes Erdős-Rényi (ER) graphs with different sizes (100, 250, and 500) and average degrees $\langle k \rangle$ (see color bar). Symbols are proportional to network size. (C) Morphospace occupation of Callaway's network model overlapped with the ER ensemble as a reference. Three network sizes (100, 250, and 500) and four connectivities ($\langle k \rangle = 2, 4, 6, 8$) are present (see *SI Appendix* for additional models). (D) The coordinates of the 125 real networks are colored according to network types listed in the key and sized proportionally to number of nodes. Sources of networks (12, 13, 53, 62–67) are detailed in *SI Appendix*. Numerical data for networks are shown in *SI Appendix*, Figs. S44 and S45. GRN, MET, LANG, NEU, ECO, TECH, and B-T stand for gene regulatory, metabolic, linguistic, neuronal, ecological, technological, and bow-tie networks. (E) Vertical box shows schematic icons of three representative systems.

structure, the plane separating hierarchy from antihierarchy ($T=0$) defines a family of symmetric structures, where the downstream path diversity is canceled by the uncertainty resulting when reversing these paths. Interestingly, when cycles are incorporated to this structure at $T=0$, the resulting structure is a bow-tie organization (Fig. 3). In this particular case, a large SCC occupies a central position within a balanced feedforward structure of inputs and outputs (47). As shown in Fig. 2A, the larger the SCC is, the lower are the values of F and O .

Null Models and Real Network Analysis

Because null models do not consider optimal designs or functional constraints, they provide good insights about the part of the morphospace where no selection pressure is at work. Fig. 2B and C shows that both homogeneous and broad random networks occupy (basically) the same region in Ω . This co-occupation, within the bow-tie plane with $T(\mathcal{G})=0$ (SI Appendix, Figs. S18–S24), shows that random graphs appear located right in the middle between hierarchical and antihierarchical structures, independently of the type of degree distribution considered. Interestingly, following the configuration model approximation (48–51), theoretical results confirm this zero-centered behavior of T and the sharp dependence of O by $\langle k \rangle$ observed in numerical simulations (SI Appendix, Figs. S15–S17). Further research in the analytical behavior of these measures would consider the prediction of F behavior. The theoretical and numerical analyses indicate that hierarchical organization of null models accounts for both bow-tie structures and feedforward sparse webs affected by $\langle k \rangle$. The analysis of different models shows that differences in the degree distribution in the models produce little impact on TFO behavior.

The theoretical and numerical analyses indicate that the hierarchical organization obtained from the null models accounts for both bow-tie structures and feedforward sparse webs. Null model analysis shows that the shape of the underlying degree distribution has little impact on the TFO behavior.

What about real nets? Here we use $N_n = 125$ real networks encompassing 13 classes of natural and artificial systems [see SI Appendix, Figs. S44 and S45 for numerical details of $\mathbf{u}(\mathcal{G})$ values]. As Fig. 2D shows, a few isolated systems reach the boundaries of Ω : a cell lineage located at $\mathbf{u}(\mathcal{G}) = (0.95, 1, 1)$ and a small social network located at $\mathbf{u}(\mathcal{G}) = (-1, 0.06, 0.09)$. However, most networks fall into four clusters.

First, a group consisting of metabolic, neural, linguistic, and some social networks is found at the lower part of the bow-tie domain, clearly embedded within the cloud of random graphs (Fig. 2D). Interestingly, randomized nets of this group show a similar behavior although with a more central position within the cloud of random nets (Fig. 2 and SI Appendix, Fig. S24). An interesting case is given by the presence of bow-tie patterns in metabolic networks (52). They display a large central cycle, much larger than that observed in their randomized counterparts (SI Appendix, Fig. S29). This likely reflects the advantage of reusing and recycling molecules. The second group placed at the $O(\mathcal{G}) \approx 1$ plane shows a narrow band of feedforward nets, including electronic circuits with $-0.2 < T(\mathcal{G}) < 0.2$ and software graphs slightly biased to negative $T(\mathcal{G})$ values. Here too the dispersal seems consistent with what is expected from very diluted random graphs (Fig. 2C). This sparseness is a consequence of engineering practices focused on reducing the wiring costs while keeping the system connected (53).

The third group displays slightly positive values of $T(\mathcal{G})$ and is composed of graphs with cycles of small size but with a predominant position at the feedforward structure giving rise to a very high $O(\mathcal{G})$ with variable $F(\mathcal{G})$. These are gene regulatory networks plus a protein kinase network. The broad range of $F(\mathcal{G})$ values is due to the variable size of modules located at the top of the structure. The special location in Ω , far from the random cloud, is caused by a small fraction of genes, the DNA-binding elements (transcription factors) located at the top of the network, which participate in cycles. Finally, the fourth group is defined by an isolated cluster of ecological flow graphs, located around $\mathbf{u}(\mathcal{G}) = (0.35, 0.45, 0.25)$. Their $T(\mathcal{G}) > 0$ values indicate a certain degree of pyramidal structure and the low $O(\mathcal{G})$ s are consistent with an important role played by loops. The special status of these networks (not shared by other webs) is consistent with the well-known picture of a trophic pyramid combined with the presence of recycling (16, 54).

The four clusters point to different scenarios pervading the origins of their hierarchical organization. One key observation is that most datasets are found within the envelope predicted by the ensembles of random graphs (Fig. 2). Because these null models do not consider optimal designs or functional traits, we conclude that, as was reported in the context of modularity (55, 56), hierarchical order may be a by-product of inevitable random fluctuations, which spontaneously generate graph correlations.

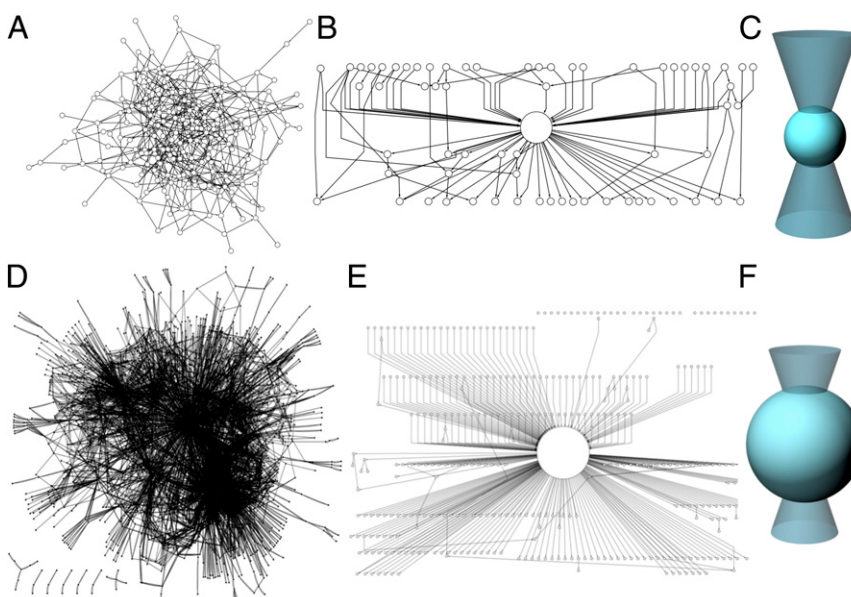


Fig. 3. Representation of null model and real bow-tie networks. (A–C) A random network $|V|=200$ and $\langle k \rangle=4$ (A), the resulting \mathcal{G}_c (B), and the respective bow-tie organization (C). (D–F) The human metabolic network (D), although nonhomogeneous and resulting from evolution, displays a similar pattern (E and F). Both graphs are close within Ω . Network layouts were generated using Cytoscape software (68).

In this context, bow-tie networks, which have been suggested to define a flexible, optimally designed, and robust type of system (22, 42), would be instead a by-product of the generation rules responsible for network growth.

Morphospace Accessibility Under Evolutionary Search

The previous results raise the question of how the voids in the morphospace need to be interpreted. To decide whether they are simply forbidden or have not been reached by evolution, we used an evolutionary search algorithm (57), which, starting from a random configuration, tries to get the points of an evenly gridded partition of the morphospace (details in *SI Appendix*). The results provide a picture of how accessible are the different regions of Ω . Very briefly, the evolutionary algorithm starts from a given set of small random graphs $\mathbf{u} \in \Omega$ belonging to the cloud of null models. Given a target point \mathbf{u}^* of Ω , these graphs are evolved by a random process of link addition and deletion with selection of networks minimizing the distance $\|\mathbf{u}_t - \mathbf{u}^*\|$. The number of nodes for every graph, $|V|=50$, remains constant in this process and graphs remain connected. Only the number of links and their distribution are affected by the evolutionary algorithm. In this way the algorithm explores the network space, approaching the desired point and sometimes reaching it. The high computational cost of this experiment makes it difficult to operate with larger networks. However, their small size provides also an advantage for the evolutionary search in the change of the network configuration because a few changes in the connections have in general a deep impact in their structure. In this way, the use of small network sizes contributes to an efficient exploration, providing a coarse-grained picture of network reachability. Further computational and theoretical efforts on the analysis of the network evolutionary behavior would contribute to a deeper understanding of the accessible regions of the *TFO* morphospace.

Fig. 4 reveals that the cloud of null models represented in Fig. 2B is easily accessible, as indicated by the dark blue color of the region. As expected, hierarchical ($T > 0$) and antihierarchical regions ($T < 0$) are quite symmetric. Deviations are due to the dispersion produced by the finite-size statistics, especially when the resulting \mathcal{G}_c become very little, by the imposition of a high number of cycles, as happens for $O=0.15$. This is the reason why, at $O=0.15$, reachability is rather heterogeneous. The solutions for this orderability are possible only by forcing the network population to exhibit a large fraction of the nodes within cycles. This constraint inevitably produces a \mathcal{G}_c with just a handful of nodes. Then, as happens for a broad number of topological measures, values of T and F are sensitive to small variations in network configurations. Such a trend is less dramatic when O increases (see $O=0.5$ and $O=0.85$ in Fig. 4) because the fraction of nodes belonging to cycles is small enough to produce a rich combination of configurations in the resulting node-weighted condensed graphs.

However, the most interesting results here concern the presence of inaccessible regions, shown here in red. Low levels of O seem to reduce the space of possible conformations. At $O=0.15$ the extremes of T and F are inaccessible under our *in silico* evolutionary experiments. Such a behavior is relaxed at $O=0.5$. Here, a large region of high reachability is observed for extreme values of T but not occupied by real networks. This may indicate that a part of Ω is accessible and yet not occupied, suggesting that the spontaneous correlations created by random fluctuations provide the source of order for free. This would give support to the role played by nonadaptive processes (58) in shaping hierarchies both in nature and in man-made systems.

Finally, an interesting trend is observed when O approaches its upper bound. The larger O is, the more reduced is the range of the possibilities of F . Close to $O=1$, only graph configurations for $F=1$ exist, coinciding with feedforward networks encompassing electronic circuits and software networks.

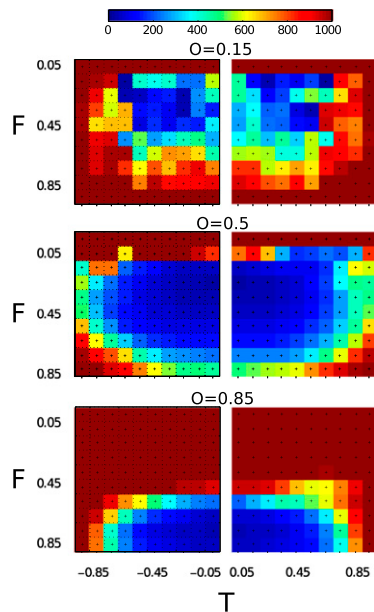


Fig. 4. Searching the possible in Ω by an evolutionary algorithm exploration (see *SI Appendix* for algorithm details). Ω was evenly spaced in 300 target points \mathbf{u}^* distributed in a partition of 10×10 of the *TF* plane and three values of $O(\mathcal{G}) = \{0.15, 0.5, 0.85\}$. Target points are labeled by crosses. Color indicates at which generation grids were acquired in an average of 250 evolutionary experiments. Blue squares indicate accessibility after a few rounds of the process. Red square indicate that they were unreachable before 10^3 iterations.

Concluding Remarks

Both biological evolution and cultural evolution operate under a number of deep constraints (59). Some of them result from the underlying rules of network growth and change, which strongly limit the repertoire of potential designs. An important question posed by evolutionary theory is the nature and relevance of such constraints in shaping the space of the possible. Our study provides a rationale for exploring the possible and the actual in complex networks under a static view dominated by causal relations among components and modules. In this context, the inclusion of functionality, dynamics, or weighted structures has not been taken into account and should be the object of further work. By defining a general space of hierarchical webs, we are able to detect the presence of a rather limited domain occupied by real and random null models. The large voids surrounding these clusters of webs (defining four major groups) are partially inaccessible and partially reachable, as shown by means of a directed evolution algorithm.

The majority of webs display a balance between integration of multiple signals and control over multiple targets under a bowtie structural pattern. The computational nature of regulatory networks and the combination of layers and cycles common to energy flows in food webs separate them from this large cluster. The matching of random and real webs in the first two clusters suggests that their hierarchical features can be accounted for from the spontaneous correlations associated to random graphs of a given degree, indicating that the observed webs are simply the most probable ones. By connecting network theory with theoretical morphology a powerful picture of complexity emerges, which allows us to both characterize hierarchical order and provide an evolutionary framework to explain how hierarchy emerges in nature. The formalism presented in this work provides a suitable framework for the quantitative approximation for the study of hierarchical organizations, and links to non-equilibrium thermodynamics could be defined in the future, attending to the similarity of certain approaches (60, 61). Further

effort in the inclusion of the strength of relations among elements from empiric data as weighted graphs would contribute to a more accurate view of the hierarchy of systems. Future work in the development of generative models for the study of the emergence of hierarchy will be of strong interest in the study of dynamics in the exploration of the limits of what is possible for natural, technological, and social organizations.

- ACKNOWLEDGMENTS.** We thank Complex Systems Laboratory members and Olaf Sporns for useful comments; Wormbase, Vladimir Batagelj, and Andrej Mrvar for the Pajek dataset; and Mark Newman for his network dataset. R.V.S. thanks D. Erwin, E. Smith, G. West, and M. Gell-Mann for useful discussions on hierarchy. The Botín Foundation, the James McDonnell Foundation, Spanish Government Grant E-28-2012-0504681 (to J.G.), the Austrian Fonds zur Förderung der Wissenschaftlichen Forschung project “Quantifying socio-economic multiplex networks in a massive multiplayer online game.” KPP23378FW (to B.C.-M.), and the Santa Fe Institute supported this work.
1. Simon HA (1962) The architecture of complexity. *Proc Am Philos Soc* 106:467–482.
 2. Mihm J, Loch CH, Wilkinson DM, Huberman BA (2010) Hierarchical structure and search in complex organizations. *Manage Sci* 56:831–848.
 3. Amaral MHR, Loch CH, Wilkinson D, Huberman BA (1996) Scaling behaviour in the growth of companies. *Nature* 379:831–848.
 4. Guimerà R, Danon L, Diaz-Guilera A, Giralt F, Arenas A (2003) Self-similar community structure in a network of human interactions. *Phys Rev E Stat Nonlin Soft Matter Phys* 68(Pt 2):065103.
 5. Valverde S, Solé RV (2007) Self-organization versus hierarchy in open-source social networks. *Phys Rev E Stat Nonlin Soft Matter Phys* 76(4 Pt 2):046118.
 6. Krugman PR (1996) Confronting the mystery of urban hierarchy. *J Jpn Int Econ* 10: 399–418.
 7. Batty M, Longley P (1994) *Fractal Cities: A Geometry of Form and Function* (Academic, San Diego).
 8. West GB, Brown JH, Enquist BJ (1997) A general model for the origin of allometric scaling laws in biology. *Science* 276(5309):122–126.
 9. Ma HW, Buer J, Zeng AP (2004) Hierarchical structure and modules in the Escherichia coli transcriptional regulatory network revealed by a new top-down approach. *BMC Bioinformatics* 5:199.
 10. Yu H, Gerstein M (2006) Genomic analysis of the hierarchical structure of regulatory networks. *Proc Natl Acad Sci USA* 103(40):14724–14731.
 11. Cosentino Lagomarsino M, Jona P, Bassetti B, Isambert H (2007) Hierarchy and feedback in the evolution of the Escherichia coli transcription network. *Proc Natl Acad Sci USA* 104(13):5516–5520.
 12. Bhardwaj N, Yan KK, Gerstein MB (2010) Analysis of diverse regulatory networks in a hierarchical context shows consistent tendencies for collaboration in the middle levels. *Proc Natl Acad Sci USA* 107(15):6841–6846.
 13. Rodríguez-Caso C, Corominas-Murtra B, Solé RV (2009) On the basic computational structure of gene regulatory networks. *Mol Biosyst* 5(12):1617–1629.
 14. Erwin DH, Davidson EH (2009) The evolution of hierarchical gene regulatory networks. *Nat Rev Genet* 10(2):141–148.
 15. Hirata H, Ulanowicz R (1985) Information theoretical analysis of the aggregation and hierarchical structure of ecological networks. *J Theor Biol* 116:321–341.
 16. Wickens J, Ulanowicz R (1988) On quantifying hierarchical connections in ecology. *J Soc Biol Struct* 11:369–378.
 17. Rodríguez-Iturbe I, Rinaldo A (1996) *Fractal River Basins: Chance and Self-Organization* (Cambridge Univ Press, Cambridge, UK).
 18. Kaiser M, Hilgetag CC, Kötter R (2010) Hierarchy and dynamics of neural networks. *Front Neuroinform* 4:112.
 19. Eldredge N (1985) *Unfinished Synthesis: Biological Hierarchies and Modern Evolutionary Thought* (Oxford Univ Press, New York).
 20. McShea DW (2001) The hierarchical structure of organisms. *Paleobiology* 27:405–423.
 21. Guimerà R, Arenas A, Diaz-Guilera A (2001) Communication and optimal hierarchical networks. *Physica A* 299:247–252.
 22. Stelling J, Sauer U, Szallasi Z, Doyle FJ, 3rd, Doyle J (2004) Robustness of cellular functions. *Cell* 118(6):675–685.
 23. Lane D (2006) *Hierarchy in Natural and Social Sciences*, ed Pumain D (Springer, Dordrecht, The Netherlands), pp 81–119.
 24. Ravasz E, Somera AL, Mongru DA, Oltvai ZN, Barabási AL (2002) Hierarchical organization of modularity in metabolic networks. *Science* 297(5586):1551–1555.
 25. Vázquez A, Pastor-Satorras R, Vespignani A (2002) Large-scale topological and dynamical properties of the Internet. *Phys Rev E Stat Nonlin Soft Matter Phys* 65(Pt 2): 066130.
 26. Trusina A, Maslov S, Minnhagen P, Sneppen K (2004) Hierarchy measures in complex networks. *Phys Rev Lett* 92(17):178702.
 27. Clauset A, Moore C, Newman MEJ (2008) Hierarchical structure and the prediction of missing links in networks. *Nature* 453(7191):98–101.
 28. Corominas-Murtra B, Rodríguez-Caso C, Goñi J, Solé R (2011) Measuring the hierarchy of feedforward networks. *Chaos* 21(1):016108.
 29. Dehmer M, Borgert S, Emmert-Streib F (2008) Entropy bounds for hierarchical molecular networks. *PLoS ONE* 3(8):e3079.
 30. Rammal R, Toulouse G, Virasoro MA (1986) Ultrametricity for physicists. *Rev Mod Phys* 58(3):765–768.
 31. Song CM, Havlin S, Makse HA (2006) Origins of fractality in the growth of complex networks. *Nat Phys* 2:275–281.
 32. Nicolis JS (1986) *Dynamics of Hierarchical Systems: An Evolutionary Approach* (Springer, London).
 33. Mones E, Vicsek L, Vicsek T (2012) Hierarchy measure for complex networks. *PLoS ONE* 7(3):e33799.
 34. Mones E (2013) Hierarchy in directed random networks. *Phys Rev E Stat Nonlin Soft Matter Phys* 87(2):022817.
 35. Niklas KJ (1994) Morphological evolution through complex domains of fitness. *Proc Natl Acad Sci USA* 91(15):6772–6779.
 36. McGhee GR (1999) *Theoretical Morphology. The Concept and Its Applications* (Columbia Univ Press, New York).
 37. Thomas RD, Shearman RM, Stewart GW (2000) Evolutionary exploitation of design options by the first animals with hard skeletons. *Science* 288(5469):1239–1242.
 38. Shoval O, et al. (2012) Evolutionary trade-offs, Pareto optimality, and the geometry of phenotype space. *Science* 336(6085):1157–1160.
 39. Schuetz R, Zamboni N, Zampieri M, Heinemann M, Sauer U (2012) Multidimensional optimality of microbial metabolism. *Science* 336(6081):601–604.
 40. Goñi J, et al. (2013) Exploring the morphospace of communication efficiency in complex networks. *PLoS ONE* 8(3):e58070.
 41. Whyte LL, Wilson AG, Wilson DM (1969) *Hierarchical Structures* (Elsevier, New York).
 42. Kitano H (2004) Biological robustness. *Nat Rev Genet* 5(1):826–837.
 43. Gross J, Yellen J (1998) *Graph Theory and Its Applications* (CRC, Boca Raton, FL).
 44. Bonchev D, Rouvray D (2005) *Complexity in Chemistry, Biology, and Ecology, Mathematical and Computational Chemistry* (Springer, Berlin).
 45. Zhao J, Yu H, Luo JH, Cao ZW, Li YX (2006) Hierarchical modularity of nested bow-ties in metabolic networks. *BMC Bioinformatics* 7:386.
 46. Corominas-Murtra B, Rodríguez-Caso C, Goñi J, Solé RV (2010) Topological re-variability and causality in feed-forward networks. *New J Phys* 12:113051.
 47. Broder A, et al. (2000) Graph structure in the web. *Comput Netw* 33:309–320.
 48. Bollobás B (1985) *Random Graphs* (Academic, London).
 49. Dorogovtsev SN, Mendes JFF, Samukhin AN (2001) Giant strongly connected component of directed networks. *Phys Rev E Stat Nonlin Soft Matter Phys* 64(2 Pt 2):025101.
 50. Newman MEJ, Strogatz SH, Watts DJ (2001) Random graphs with arbitrary degree distributions and their applications. *Phys Rev E Stat Nonlin Soft Matter Phys* 64(2 Pt 2): 026118.
 51. Newman MEJ (2010) *Networks: An Introduction* (Oxford Univ Press, New York).
 52. Ma HW, Zeng AP (2003) The connectivity structure, giant strong component and centrality of metabolic networks. *Bioinformatics* 19(11):1423–1430.
 53. Cancho RF, Janssen C, Solé RV (2001) Topology of technology graphs: Small world patterns in electronic circuits. *Phys Rev E Stat Nonlin Soft Matter Phys* 64(4 Pt 2):046119.
 54. Allesina S, Bodini A, Bondavalli C (2005) Ecological subsystems via graph theory: The role of strongly connected components. *Oikos* 110(1):164–176.
 55. Guimerà R, Sales-Pardo M, Amaral LAN (2004) Modularity from fluctuations in random graphs and complex networks. *Phys Rev E Stat Nonlin Soft Matter Phys* 70(2 Pt 2):025101.
 56. Solé RV, Valverde S (2008) Spontaneous emergence of modularity in cellular networks. *J R Soc Interface* 5(18):129–133.
 57. Marín J, Solé RV (1999) Macroevolutionary algorithms: A new optimization method on fitness landscapes. *IEEE Trans Evol Comput* 3(4):272–286.
 58. Lynch M (2007) The evolution of genetic networks by non-adaptive processes. *Nat Rev Genet* 8(10):803–813.
 59. Solé RV, et al. (2013) The evolutionary ecology of technological innovations. *Complexity* 18(4):15–27.
 60. Rinaldo A, et al. (1996) Thermodynamics of fractal networks. *Phys Rev Lett* 76: 3364–3367.
 61. Wissner-Gross AD, Freer CE (2013) Causal entropic forces. *Phys Rev Lett* 110(16):168702.
 62. Goñi J, Corominas-Murtra B, Solé RV, Rodríguez-Caso C (2010) Exploring the randomness of directed acyclic networks. *Phys Rev E Stat Nonlin Soft Matter Phys* 82(6 Pt 2):066115.
 63. White JG, Southgate E, Thomson JN, Brenner S (1986) The structure of the nervous system of the nematode *Caenorhabditis elegans*. *Philos Trans R Soc Lond B Biol Sci* 314(1165):1–340.
 64. Jeong H, Tombor B, Albert R, Oltvai ZN, Barabási AL (2000) The large-scale organization of metabolic networks. *Nature* 407(6804):651–654.
 65. Ma H, Zeng AP (2003) Reconstruction of metabolic networks from genome data and analysis of their global structure for various organisms. *Bioinformatics* 19(2):270–277.
 66. Ma H, et al. (2007) The Edinburgh human metabolic network reconstruction and its functional analysis. *Mol Syst Biol* 3:135.
 67. Valverde S, Solé RV (2005) Logarithmic growth dynamics in software networks. *Europhys Lett* 72:858–864.
 68. Smoot ME, Ono K, Ruscheinski J, Wang PL, Ideker T (2011) Cytoscape 2.8: New features for data integration and network visualization. *Bioinformatics* 27(3):431–432.

Hierarchy in complex networks: the possible and the actual: Supporting Information

Bernat Corominas-Murtra * † ‡, Joaquín Goñi §, Ricard V. Solé * † ¶ and Carlos Rodríguez-Caso * †

*Institució Catalana per a la Recerca i Estudis Avançats-Complex Systems Lab, Universitat Pompeu Fabra, 08003 Barcelona, Spain

, †Institut de Biología Evolutiva, (CSIC-UPF), Psg. de la Barceloneta 37, 08003 Barcelona, Spain

, ‡Section for Science of Complex Systems, Medical University of Vienna, Spitalgasse 23, 1090 Vienna, Austria

, § Department of Psychological and Brain Sciences, Indiana University, Bloomington IN 47405, USA

, and ¶Santa Fe Institute, 1399 Hyde Park road, Santa Fe NM 87501, USA

Proceedings of the National Academy of Sciences of the United States of America

Contents

Introduction

Structure of the text	1
The fundamentals of hierarchy	1
Postulates of Hierarchy	1

Graph definitions

Directed Graphs	2
Directed Acyclic Graphs	2
Condensation: Obtaining a DAG from any directed graph	3
<i>Node-weighted</i> condensed graph	3
Dissection of the layers of the graph	4

The Coordinates of Hierarchy

Orderability, O	5
Feedforwardness, F	5
Treeness, T	6
Backwards entropy	6
Forward entropy	7
Treeness	7
The coordinates of hierarchy for directed graphs	7
Analytical estimates for random graphs	9
T in random directed graphs	9
O in random directed graphs	10
F in random directed graphs	11

Analysis of Networks

Model Networks	12
Directed ER graphs	12
Directed Callaway graphs	13
Directed BA graphs	13
Real Networks	13
Network dataset	14
Randomization Methods	15
Confronting real data with their randomized counterparts	16
The accessibility of the Morphospace: Evolution	18

Software availability

Real Nets Analysis: Figures	19
Numerical data from real and randomized networks	21

Introduction

This supporting material presents in a self-contained way the conceptual issues that lead us to the rigorous formalization of hierarchy in complex networks. Although some of these concepts can be found in standard handbooks on graph theory -for example [1]-, we present all them from scratch in order to

provide the reader with a consistent and clear mathematical apparatus. The aim is to remove any inconsistency in notation when introducing original concepts. The type of object studied here is any kind of *connected* directed graph, i.e., any directed graph composed by a single component. Although the formalism could be applied over graph structures consisting in more than a single component -as usually happens when working with random graphs- we assume that unconnected components have no causal relation of any kind and, therefore, the concept of hierarchy loses any meaning. As we shall see, the possibility to relate parts of the system by means of the topological information is basic for our definition of hierarchy.

Structure of the text. The text is structured as follows: First we present in an axiomatic way the features a given system based on relations among objects must hold in order to be considered *perfectly hierarchical*. Deviations from this perfect configuration have to be properly quantified, giving rise to the three coordinates of the hierarchy. Then, we provide the basis to work with, revising several basic definitions of directed graphs and some of their most salient properties. We focus our attention on the condensation operation and on the layered structure of the resulting condensed graph. Basic definitions are followed by the proper definition of the hierarchy coordinates. Such definitions are detailed and described with the aim of conveying the reader the flavour and intuitions that underlie them. We end this section with the analytical estimates of the presented coordinates in totally disordered graphs. Once the formal framework is properly described we explore the regions of the defined morphospace occupied by model networks. This section is followed by the list of studied networks and the randomization methods we used to explore the relevance of the observed results. It is important to stress that the rigorous and systematic confrontation of real data with their randomized counterparts elucidates much of the possible origins of the observed patterns. Finally, we explore the space of possible hierarchical configurations through an evolutionary algorithm whose rules are described in detail.

The fundamentals of hierarchy. What are the mathematical features of a system called *hierarchical*? Hierarchy is a property about how system's components are interrelated. We state, as a definition, that such pattern of relations is hierarchical if it satisfies the following postulates.

Postulates of Hierarchy

The *perfectly hierarchical system* will have the following three properties:

- *order*,
- *reversibility* and
- *pyramidal structure*.

Let us be more precise. Suppose we have a set $A = \{a_1, \dots, a_n\}$ and a set relation $R \subset A \times A$ ¹. Let $T(R)$ be the *transitive closure* of R ², we will say that R is *hierarchical* if R has the following properties:

- *order*,

$$\text{if } \langle a_i, a_k \rangle \in T(R), \text{ then } \langle a_k, a_i \rangle \notin T(R)$$

(There are no cyclic relationships: we can **order** the elements³)

- *reversibility*

$$\text{if } \langle a_i, a_k \rangle \in R \text{ and } \langle a_j, a_k \rangle \in R, \text{ then } a_i = a_j$$

(There is only one commander for any commanded: The chain of commands is **reversible**.)

- *pyramidal structure*

a) if $\langle a_i, a_k \rangle \in R$ then, $\exists a_j \neq a_k$ such that $\langle a_i, a_j \rangle \in R$ (*A commander commands more than a single element.*)

b) $(\exists! a_k \in A)$ such that $(\forall a_i \in A \setminus \{a_k\})(\langle a_k, a_i \rangle \in T(R))$ (*There is only a single element which is not commanded by another element.*)

c) Let J_i be the set of commanders of element a_i , i.e.: $J_i = \{a_k \in A : \langle a_k, a_i \rangle \in T(R)\}$ If $a_i, a_j \in A$ are such that $\nexists a_k \in A$ such that $\langle a_i, a_k \rangle \in R$ or $\langle a_j, a_k \rangle \in R$, then $|J_i| = |J_j|$. (*All the elements of the bottom are subjected to a chain of commands of the same length. These last properties give the pyramidal structure of R*)

It is straightforward to realize that the directed, inverted tree in which all the arrows go *downwards* starting from a single root naturally emerges as the graphical description of the perfect hierarchical system -see figure (1). The rigorous proof of this statement is given as a lemma in section *The Coordinates of Hierarchy* when the appropriate formalism is developed.

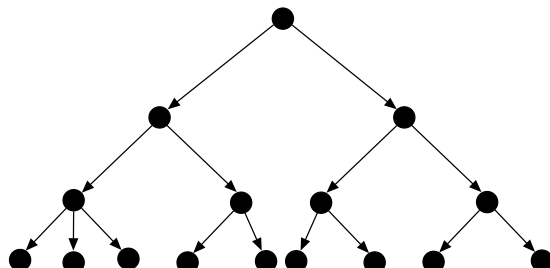


Fig. 1. A possible chart of relations depicting a perfectly hierarchical system.

The measure of hierarchy must properly quantify the deviations from this perfect structure, considering these three postulated properties.

Graph definitions

The whole set of relationships between elements of the systems under scrutiny define a *directed graph*. In any directed graph, links describe some kind of causal relation between two elements of the set which is considered relevant for the system. We thus begin revising several facts about directed graphs. These basic notions can be found in any standard textbook on graph theory, like [1].

Directed Graphs. Let $\mathcal{G}(V, E)$ be a directed graph, being $V = \{v_1, \dots, v_n\}$, $|V| = n$, the set of nodes, and $E =$

$\{\langle v_k, v_i \rangle, \dots, \langle v_j, v_l \rangle\}$ the set of arcs -where the order, $\langle v_k, v_i \rangle$ implies that there is an arc in the following direction: $v_k \rightarrow v_i$. Given a node $v_i \in V$, the number of outgoing links, to be written as $k_{out}(v_i)$, is called the *out-degree* of v_i , and the number of ingoing links of v_i is called the *in-degree* of v_i , written as $k_{in}(v_i)$. The *adjacency matrix* of a given graph \mathcal{G} , $\mathbf{A}(\mathcal{G})$ is a $n \times n$ matrix where $A_{ij}(\mathcal{G}) = 1 \leftrightarrow \langle v_i, v_j \rangle \in E$; and $A_{ij}(\mathcal{G}) = 0$ otherwise. Through the adjacency matrix, k_{in} and k_{out} are computed as

$$k_{in}(v_i) = \sum_{j \leq n} A_{ji}(\mathcal{G}); \quad k_{out}(v_i) = \sum_{j \leq n} A_{ij}(\mathcal{G}). \quad [1]$$

A *path* from node $v_i \in V$ to node $v_j \in V$, $\pi_k(v_i, v_j)$ in a directed graph is an alternated sequence of nodes and links:

$$\pi_k(v_i, v_j) = v_i, \langle v_i, v_j \rangle, v_j, \dots, v_\ell, \langle v_\ell, v_j \rangle, v_j$$

such that

$$\langle v_i, v_j \rangle, \dots, \langle v_\ell, v_j \rangle \in E.$$

(The k subscript is due to the possible presence of more than a single path from v_i to v_j). The *length* of a path, $\ell(\pi_k(v_i, v_j))$ is the number of edges appearing in the sequence. We observe that some edges can appear twice or more in the sequence. In that case, we take into account all appearances of the edge. Since a path $\pi_k(v_i, v_j)$ is an alternating sequence of nodes and links, it seems natural to define two sets: $v(\pi_k(v_i, v_j))$ as the set of all nodes present in the path and $e(\pi_k(v_i, v_j))$, the set of all edges present in the path. Then we define the set $\Pi(\mathcal{G})$ as the (possibly infinite) set of all paths that can be defined in \mathcal{G} .

A *cycle* in a directed graph is the subgraph formed by the edges and nodes defining a path which begins and ends in the same node, i.e, if

$$v_i, \langle v_i, v_j \rangle, v_j, \dots, v_\ell, \langle v_\ell, v_i \rangle, v_i$$

such that $\langle v_i, v_j \rangle, \dots, \langle v_\ell, v_i \rangle \in E$. The set of cycles of a given graph is $\mathcal{C}(\mathcal{G}) = \{C_1, \dots, C_k\}$. If $C_k \in \mathcal{C}(\mathcal{G})$ is maximal, i.e.,

$$\nexists C_i \in \mathcal{C}(\mathcal{G}) : C_k \subset C_i, \quad [2]$$

then, C_k is called a *Strongly Connected Component*, hereafter *SCC*. We will refer to the set of *SCC*'s as $\Sigma(\mathcal{G}) = \{S_1, \dots, S_\ell\}$. Since every *SCC* is itself a subgraph, we can refer to it as $S_k = S_k(V_{S_k}, E_{S_k})$, where V_{S_k} , E_{S_k} are the nodes and the edges of S_k , respectively.

The *underlying graph* of a given directed graph \mathcal{G} , to be written as \mathcal{G}^u , is the undirected graph $\mathcal{G}^u(V, E^u)$ obtained by substituting all arcs of E , $\langle v_i, v_k \rangle, \langle v_j, v_s \rangle, \dots$ by undirected edges giving the set $E^u = \{\{v_i, v_k\}, \{v_j, v_s\}, \dots\}$. A directed graph \mathcal{G} is said to be *connected* if for any pair of nodes $v_i, v_l \in V$ there is a finite, undirected path linking them; i.e., a finite sequence

$$v_i, \{v_i, v_k\}, v_k, \dots, v_s, \{v_m, v_\ell\}, v_\ell$$

where $\{v_i, v_k\}, \dots, \{v_m, v_\ell\} \in E_u$. Notice that now the links are depicted by unordered pairs, therefore $\{v_i, v_k\} = \{v_k, v_i\}$.

¹Elements of a given set relation are *ordered pairs* e.g., $R = \{\langle a_i, a_j \rangle, \dots, \langle a_k, a_\ell \rangle\}$, being $a_i, a_j, a_k, a_\ell \in A$. When we write $\langle a_k, a_\ell \rangle$ we say that a_k is related to a_ℓ through relation R , which can also be written as $a_k Ra_\ell$. Notice that $(\langle a_k, a_\ell \rangle \in R) \nRightarrow (\langle a_\ell, a_k \rangle \in R)$ necessarily. If this happens, this means that $a_k Ra_\ell$ and $a_\ell Ra_k$, and a_k, a_ℓ form an *unordered pair*, represented by $\{a_k, a_\ell\}$

²Given a set A , The transitive closure of a relation $R \subseteq A \times A$ is the minimal transitive relation R' such that $R \subseteq R'$. See [2, 3] or [1].

³In this case, we impose that $T(R)$ is a *strict partial order*. $K \in A \times A$ is a strict partial order if it is i) $(\forall a_i \in A)(\langle a_i, a_i \rangle \notin K)$ (non-reflexive) ii) $(\langle a_i, a_k \rangle \in K) \Rightarrow (\langle a_k, a_i \rangle \notin K)$ (antisymmetric) and iii) $[(\langle a_i, a_k \rangle \in K) \wedge (\langle a_k, a_j \rangle \in K)] \Rightarrow (\langle a_i, a_j \rangle \in K)$ (transitive).

Given a graph $\mathcal{G}(V, E)$, a *component* γ_j is a maximal subgraph of \mathcal{G} by which, for every pair of nodes v_k, v_i belonging to it there is an undirected, finite path linking them. We refer to the set of components of \mathcal{G} as

$$\Gamma(\mathcal{G}) = \{\gamma_1, \dots, \gamma_k\}.$$

It turns out that a connected graph has only one component, the graph itself. In general, we will work with connected graphs. It is worth to note that, connectedness may be lost during a randomization process but, as we shall see in section *Real Networks*, the randomization methods we use respect the structure of components of the graph -i.e., connectedness if it be.

Directed Acyclic Graphs. A *directed acyclic graph* or *feedforward graph* -hereafter, *DAG*- is a directed graph characterized by the absence of cycles. The first consequence of the absence of cycles is the non-existence of infinite paths within -a finite- \mathcal{G} . *DAGs* have been also referred to as *ordered graphs* because it is always possible to *topologically sort* a *DAG* [1]. A topological sorting consists in numbering all the nodes v_1, v_2, \dots, v_n in such a way that arcs always point to nodes having higher numerical label than their origin, i.e., for any pair v_k, v_j such that $k > j$, then

$$\langle v_k, v_j \rangle \notin E.$$

This property will be crucial to justify the link between hierarchy, order and causal relation. This sorting implies that a *DAG* can represent a more or less entangled structure of interconnected causal processes.

We stress in the analogy between order theory and *DAG* structures by defining following set:

$$M = \{v_i \in V : k_{in}(v_i) = 0\}, \quad [3]$$

to be named the set of *maximal nodes* of \mathcal{G} . In a complementary way, one can define the set of nodes μ as

$$\mu = \{v_i \in V : k_{out}(v_i) = 0\}, \quad [4]$$

which will be referred to as the set of *minimal nodes* of \mathcal{G} .

The set of all paths π_1, \dots, π_s , from M to μ is indicated as $\Pi_{M\mu}(\mathcal{G})$. Given a node $v_i \in \mu$, the set of all paths from M to v_i is written as

$$\Pi_{M\mu}(v_i) \subseteq \Pi_{M\mu}(\mathcal{G}). \quad [5]$$

We observe that the length of the *longest* path of a finite *DAG* is always bounded. We will refer to this numerical value as $L(\mathcal{G})$ which, taking into account the properties of the powers of the adjacency matrix, can be straightforwardly obtained⁴:

$$L(\mathcal{G}) = \max\{k : (\exists v_i, v_j \in V : (\mathbf{A}^k(\mathcal{G}))_{ij} \neq 0)\}. \quad [6]$$

A special type of *DAG* is to be defined now, since, as we will show below, depicted the perfect hierarchy. A *directed tree* in which *all the leafs have the same length* is a *DAG* with $|M(\mathcal{G})| = 1$ in which all elements but the one in M have $k_{in} = 1$, either $k_{out} = 0$ or $k_{out} \geq 2$ and in which $\forall v_i, v_j \in \mu(\mathcal{G})$, if $v_k \in M$, then $\ell(\pi(v_k, v_i)) = \ell(\pi(v_k, v_j))$ -the leafs are all paths going from M to μ . See figure (1) for an example of this kind of graph.

Let us now take the set-theoretic framework used at the beginning of this document and replace A by V (the set of nodes) and R by $E \in V \times V$ (the set of links). Now we have a graph representation of the kind of relations that display a perfect hierarchical organization. It turns out that the type of graph defined above satisfies all the postulates defined in the graphical representation of a perfect hierarchical system. Let us state is as a formal lemma:

Lemma: Under the hallmark described (see section 'Postulates of Hierarchy'), the kind of graph \mathcal{G} depicting the perfect hierarchy is a directed tree in which all the leafs have the same length.

Proof: By the *order* property, \mathcal{G} has no cycles. By the *reversibility* property the graph nodes of the graph have either $k_{in} = 0$ or $k_{in} = 1$. By the *pyramidal* property **a**) the nodes have either $k_{out} = 0$ or $k_{out} \geq 2$. By the *pyramidal* property **b**) the graph is connected and $|M(\mathcal{G})| = 1$ and by the *pyramidal* property **c**), if $v_k \in M$, then $\forall v_i, v_j \in \mu(\mathcal{G})$, then $\ell(\pi(v_k, v_i)) = \ell(\pi(v_k, v_j))$ (notice that there is only one path to go from $v_k \in M(\mathcal{G})$ to a given $v_i \in \mu(\mathcal{G})$). Therefore, \mathcal{G} is *directed tree* in which *all the leafs have the same length*.

Now that we have the mathematical characterization of the perfectly hierarchical graph, we restart the conceptual presentation that will help us to properly evaluate deviations from the ideal graph.

Condensation: Obtaining a *DAG* from any directed graph

Now we consider again the wide class of directed graphs, not only *DAGs*. Let $\Sigma(\mathcal{G}) = \{S_1, \dots, S_k\}$ be the set of *SCCs*. We will build the *condensed graph* of \mathcal{G} , to be referred to as \mathcal{G}_C , in which every *SCC* is merged into a single node, maintaining the links that connect a node of such *SCC* with nodes out of such *SCC*. More formally,

$$V_C = \Sigma(\mathcal{G}) \cup \left[V \setminus \left(\bigcup_{\Sigma(\mathcal{G})} V_{S_j} \right) \right],$$

i.e., nodes of \mathcal{G}_C are either *SCCs* of \mathcal{G} or nodes that do not belong to any *SCC* of \mathcal{G} . Consistently, edges on E_C connect nodes of V_C in such a way that $(\forall v_i, v_j \in V_C) \langle v_i, v_j \rangle \in E_C$ if and only if:

$$\begin{cases} \langle v_i, v_j \rangle \in E. \\ (v_i = S_k \in \Sigma(\mathcal{G}), v_j \in V) \wedge (\exists v_\ell \in S_k) : (\langle v_\ell, v_j \rangle \in E). \\ (v_i = S_k \in \Sigma(\mathcal{G}), v_j = S_\ell \in \Sigma(\mathcal{G})) \wedge \\ \quad \wedge (\exists v_m \in S_k, \exists v_s \in S_\ell) : (\langle v_m, v_s \rangle \in E); \text{ for } k \neq \ell. \end{cases}$$

It turns out that, by definition, \mathcal{G}_C is a *DAG*.

Below we have an example of the condensation operation, step by step. We have a graph \mathcal{G} (left). We then identify the *SCCs* of \mathcal{G} (center) and collapse all nodes belonging to a *SCC* in a single node, thus obtaining \mathcal{G}_C (right):

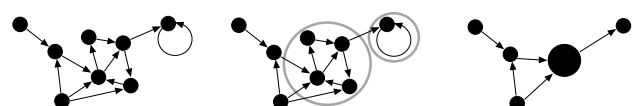


Fig. 2. The three stages of the condensation algorithm.

Notice, as illustrated in figure (2) that \mathcal{G}_C is a *DAG*, as expected.

Node-weighted condensed graph

A conceptual step beyond the condensed graph is the *node-weighted* condensed graph. All the computations presented in this paper will be performed over such a graph. Let us formally describe it: In this graph, a weight α_i is assigned to

⁴This contrasts with the case of a graph containing cycles, where, even in the case of being finite, cycles allow the presence of paths of infinite length.

every node $v_i \in V_C$ in the following way:

$$\alpha_i = \begin{cases} 1 \Leftrightarrow v_i \in V \cap V_C \\ |S_i| \Leftrightarrow v_i \in \Sigma(\mathcal{G}). \end{cases}$$

Therefore, the sequence of

$$\Lambda = \alpha_1, \dots, \alpha_{|V_C|}$$

will be the sequence of weights of \mathcal{G}_C . Clearly,

$$\sum_{i \leq |V_C|} \alpha_i = |V|.$$

In plain words, α_i accounts for the number of nodes belonging to V represented by a single node in V_C . In the forthcoming example we detail the obtaining of such a graph from a given directed graph. We have the graph -left-; then, we identify its *SCCs* -center- and, then, -right- we label the nodes of \mathcal{G}_C with their corresponding α 's:

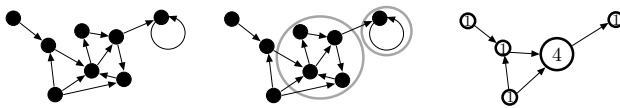


Fig. 3. Obtaining the node-weighted condensed graph \mathcal{G}_C .

Dissection of the layers of the graph

The objective of this section is to rigorously define the dissection in layers of a given *DAG*. The non-cyclic nature of such graph structures enables us to define a finite set of layers. Layers can be identified through a *backward* or *bottom up leaf removal* (LR_b) algorithm or through a *forward* or *top down leaf removal* (LR_f) algorithm⁵. Although LR_f and LR_b algorithms identify the same number of layers, the specific composition of every layer is not necessarily the same. In addition, using these two algorithms, we can build two sets of subgraphs by successively removing layers of the *DAG*. As we shall see, these two sets will be very useful to derive the proposed measure of hierarchy.

Accordingly, we define two partitions of V_C , $W = \{\omega_1, \dots, \omega_m\}$ and $\tilde{W} = \{\tilde{\omega}_1, \dots, \tilde{\omega}_m\}$. The number of layers relates to $L(\mathcal{G}_C)$ -see equation (6)- as follows:

$$|W| = |\tilde{W}| = L(\mathcal{G}_C) + 1.$$

The members of such partitions are the nodes defining the layers of the *DAG*, computed by either a LR_b or LR_f algorithm -depending on which partition we generate, either W or \tilde{W} , respectively. Specifically, using the bottom up approach -i.e., using a LR_b algorithm- the first member of such partition is defined as the following subset of nodes:

$$\omega_1 = \{v_i \in V_C : k_{out}(v_i) = 0\}$$

and, using the top-down approach -i.e., using a LR_f algorithm- the first member is defined as,

$$\tilde{\omega}_1 = \{v_i \in V_C : k_{in}(v_i) = 0\}.$$

Clearly, $\omega_1 = \mu$ and $\tilde{\omega}_1 = M$. With the above subsets of V_C we can define the graphs $\mathcal{G}_1(V_1, E_1)$, and $\tilde{\mathcal{G}}_1(\tilde{V}_1, \tilde{E}_1)$ in the following way:

$$V_1 = V_C \setminus \omega_1; \quad E_1 = E_C \setminus \{\langle v_i, v_k \rangle : v_k \in \omega_1\}$$

and

$$\tilde{V}_1 = V_C \setminus \tilde{\omega}_1; \quad \tilde{E}_1 = E_C \setminus \{\langle v_i, v_k \rangle : v_i \in \tilde{\omega}_1\}.$$

respectively. Similarly, we build ω_2 and $\tilde{\omega}_2$ as:

$$\begin{aligned} \omega_2 &= \{v_i \in V_1 : k_{out}(v_i) = 0\}, \\ \tilde{\omega}_2 &= \{v_i \in \tilde{V}_1 : k_{in}(v_i) = 0\}. \end{aligned}$$

which, in turn, enables us to derive V_2 , E_2 , \tilde{V}_2 and \tilde{E}_2 :

$$\begin{aligned} V_2 &= V_1 \setminus \omega_2; & E_2 &= E_1 \setminus \{\langle v_i, v_k \rangle : v_k \in \omega_2\} \\ \tilde{V}_2 &= \tilde{V}_1 \setminus \tilde{\omega}_2; & \tilde{E}_2 &= \tilde{E}_1 \setminus \{\langle v_i, v_k \rangle : v_i \in \tilde{\omega}_2\}. \end{aligned}$$

In the general case, if $V_0 = \tilde{V}_0 = V_C$,

$$\begin{aligned} \ell &= V_{\ell-1} \setminus \omega_\ell; & E_\ell &= E_{\ell-1} \setminus \{\langle v_i, v_k \rangle : v_k \in \omega_\ell\}. \\ \tilde{\ell} &= \tilde{V}_{\ell-1} \setminus \tilde{\omega}_\ell; & \tilde{E}_\ell &= \tilde{E}_{\ell-1} \setminus \{\langle v_i, v_k \rangle : v_i \in \tilde{\omega}_\ell\}, \end{aligned}$$

where

$$1 \leq \ell \leq L(\mathcal{G}_C).$$

It is worth to note that

$$E_{L(\mathcal{G}_C)} = \tilde{E}_{L(\mathcal{G}_C)} = \emptyset,$$

and that

$$V_{L(\mathcal{G}_C)} \subseteq M; \quad \tilde{V}_{L(\mathcal{G}_C)} \subseteq \mu.$$

The two previous sequences of subgraphs can be ordered by inclusion, namely

$$G_{L(\mathcal{G}_C)} \subset \dots \subset G_1 \subset \mathcal{G}_C,$$

and

$$\tilde{G}_{L(\mathcal{G}_C)} \subset \dots \subset \tilde{G}_1 \subset \mathcal{G}_C.$$

The dissection of \mathcal{G}_C in the above described two sequences of subgraphs will enable us to exhaustively explore the role of all layers in the further hierarchy measure. We finally define the set $\mathcal{W}(\mathcal{G})$, containing the graph \mathcal{G}_C and all non-empty subgraphs obtained by means of the application of a leaf removal algorithm (either bottom up or top down) and which contain at least one link:

$$\mathcal{W}(\mathcal{G}) = \{\mathcal{G}_C, \tilde{G}_{L(\mathcal{G}_C)-1}, \dots, \tilde{G}_1, G_{L(\mathcal{G}_C)-1}, \dots, G_1\}. \quad [7]$$

It is not difficult to check that

$$|\mathcal{W}(\mathcal{G})| = 2L(\mathcal{G}_C) - 1.$$

Let us provide an example in figure (4): Starting from a *DAG* (left), we identify the layers $\omega_1, \dots, \omega_5$ using a LR_b algorithm (center), and the layers $\tilde{\omega}_1, \dots, \tilde{\omega}_5$ using a LR_f algorithm (right):

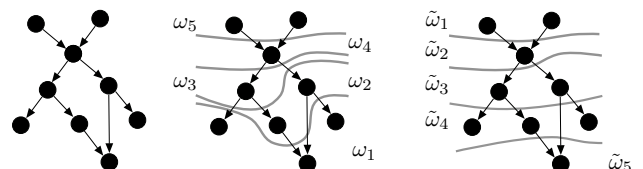


Fig. 4. The LR algorithms and the identification of layers. In this case, $|W| = 5$ and $L(\mathcal{G}) = 4$.

Furthermore, we can obtain the sequence of graphs ordered by inclusion $\mathcal{G}, \mathcal{G}_1, \dots, \mathcal{G}_4$ -notice that the last graph consists of two isolated nodes:

⁵A LR_f algorithm works as follows: Given a *DAG* \mathcal{G} , at every iteration we remove the nodes having $k_{in} = 0$ until there is no node to remove. The set of nodes removed at every iteration define a layer of the *DAG*. It is straightforward that the number of steps needed is $L(\mathcal{G}) + 1$ and so is the number of layers. A LR_b algorithm works exactly in the same way, but removing nodes having $k_{out} = 0$. The interested reader can go to [4, 5].

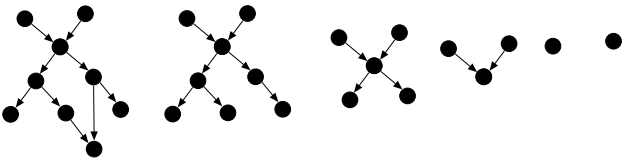


Fig. 5. The sequence of subgraphs $\mathcal{G}, \mathcal{G}_1, \dots, \mathcal{G}_4$.

And the sequence of graphs ordered by inclusion $\mathcal{G}, \tilde{\mathcal{G}}_1, \dots, \tilde{\mathcal{G}}_4$:

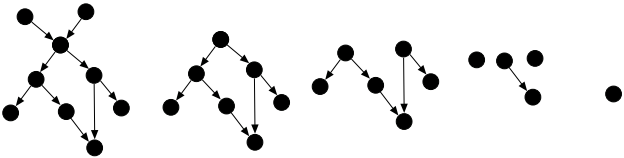


Fig. 6. The sequence of subgraphs $\mathcal{G}, \tilde{\mathcal{G}}_1, \dots, \tilde{\mathcal{G}}_4$.

The Coordinates of Hierarchy

This section is devoted to the formalization of a quantitative descriptor of hierarchy. Such a descriptor is defined from three hierarchy coordinates. These three coordinates are: *Orderability* (O), *Feedforwardness* (F) and *Treeness* (T). Thus, any directed graph will define a point in such space, described as follows:

$$\mathbf{u}(\mathcal{G}) \equiv (T(\mathcal{G}), F(\mathcal{G}), O(\mathcal{G})).$$

From the coordinates of $\mathbf{u}(\mathcal{G})$ we can extract information about the structure of the net under the conceptual background of hierarchy presented in section *Postulates of Hierarchy* based on the concepts of *order*, *reversibility* and *pyramidal structure*. Through the values of these coordinates we must be able to identify and properly quantify deviations from such an ideal behavior. As we shall see, such three components naturally arise as long as we go in depth in our inquiry for a hierarchy estimator. The order $x = T, y = F, z = O$ derives from clarity issues related to the visualization. For the sake of clarity in the exposition, however, the order of the sections in which we present such measures will not follow such T, F, O structure. Instead, we define the coordinates in such a way that we go from the simplest (O) to the most complex one (T).

We are now ready to define the coordinates of hierarchy.

Orderability, O . This is the z coordinate of $\mathbf{u}(\mathcal{G})$.

The *Orderability*, O , of the graph \mathcal{G} is the fraction of nodes not belonging to any cycle -which are, by definition, non-orderable structures. In a more formal way, let \mathcal{G} be a directed graph and \mathcal{G}_C be its condensed counterpart. The orderability of the graph $O(\mathcal{G})$ is defined as:

$$O(\mathcal{G}) = \frac{|\{v_i \in V_C \cap V\}|}{|V|}. \quad [8]$$

In terms of the node-weighted condensed graph, we can rewrite the above expression as:

$$O(\mathcal{G}) = \frac{|\{v_i \in V_C : \alpha_i = 1\}|}{|V|}.$$

Let us provide an example: In the graph depicted below (left), $|V| = 7$, $|V_C| = 5$ (right). The grey circle depicts a condensed *SCC*. $|\{v_i \in V_C \cap V\}| = 4$, therefore, $O(\mathcal{G}) = 4/7$:

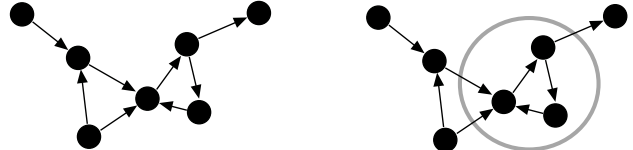


Fig. 7. Computing the orderability of the graph.

This is a raw indicator of the fraction of the net that can be ordered. A tree or, more generally, a feed-forward network will display $O(\mathcal{G}) = 1$, in agreement to their orderable nature. In contrast, a network which is totally cyclical would display $O(\mathcal{G}) = 0$.

Feedforwardness, F . This is the y coordinate of $\mathbf{u}(\mathcal{G})$.

Beyond the nodes than can be ordered, now we want to know the impact of the non-orderable regions of the graph over the potential causal paths described by it. In raw words, where, within the causal flow, we find the non-orderable regions. This is captured by the so-called *FeedForwardness*, $F(\mathcal{G})$, a measure centered on the paths of the graph \mathcal{G}_C beginning in the set of maximal nodes, M -see equations (3, 4) and (5). Specifically, for every path going from M to $V_C \setminus M$ ⁶, we define a function, F , which evaluates the quotient between the number of nodes and the overall weight of the path. To cover all nodes of the graph, the numerical value of the coordinate will be averaged over the sequence of graphs obtained when applying a LR_b algorithm. If \mathcal{G}_C is finite both M and $V \setminus M$ are finite and we can safely compute averages of these observables.

To put the things in a more concrete way, let \mathcal{G} be a graph and \mathcal{G}_C its condensed counterpart. If $\pi_k \in \Pi_{M\mu}(\mathcal{G}_C)$, we define the function F of π_k , $F(\pi_k)$, as:

$$F(\pi_k) \equiv \frac{|v(\pi_k)|}{\sum_{v_i \in v(\pi_k)} \alpha_i}.$$

For example, if we take the graph studied above and we choose the highlighted path, to be named π_j :

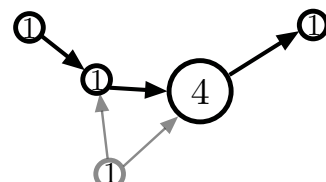


Fig. 8. Orderable fraction of a given path.

we have that $F(\pi_j) = \frac{4}{7}$.

To compute the overall average we then build the function g :

$$g(\mathcal{G}) = \sum_{\pi_i \in \Pi_{M\mu}(\mathcal{G}_C)} F(\pi_i),$$

⁶In the forthcoming lines, $M \equiv M(\mathcal{G}_C)$, $\mu \equiv \mu(\mathcal{G}_C)$, unless the contrary is indicated.

and we compute $g(\mathcal{G}_1), \dots, g(\mathcal{G}_{L(\mathcal{G})-1})$ -see section *Dissection of the layers of the graph* for the definition of \mathcal{G}_i 's:

$$g(\mathcal{G}_k) = \sum_{\pi_i \in \Pi_{M\mu}(\mathcal{G}_k)} F(\pi_i)$$

We finally average over all \mathcal{G} 's and \mathcal{G}_C , skipping $\mathcal{G}_{L(\mathcal{G})}$ because, by its very definition, this graph has no paths:

$$F(\mathcal{G}) = \frac{g(\mathcal{G}_C) + \sum_{k < L(\mathcal{G}_C)} g(\mathcal{G}_k)}{|\Pi_{M\mu}(\mathcal{G}_C)| + \sum_{k < L(\mathcal{G}_C)} |\Pi_{M\mu}(\mathcal{G}_k)|}. \quad [9]$$

And, for the sake of consistency, if the graph consists in a single node,

$$(|V| = 1) \Rightarrow (F(\mathcal{G}) = 0).$$

The interested reader can check that, with equation (9), we cover all paths from M to $V \setminus M$.

Again, we will find $F(\mathcal{G}) = 1$ in DAGs, as well as $F(\mathcal{G}) = 0$ in networks consisting of a single strongly connected component. The combination of $O(\mathcal{G})$ and $F(\mathcal{G})$ tells us how are cycles located within the net and the impact they have in the order of the structure. The combination of $O(\mathcal{G})$ and $F(\mathcal{G})$, thus, provides us interesting information on how the net is globally organized.

Treeness, T. This is the x coordinate of $\mathbf{u}(\mathcal{G})$.

This measure accounts for the *reversibility* and the *pyramidal structure*. The forthcoming coordinate is of information-theoretic nature and can only be computed over the condensed graph \mathcal{G}_C , since it can only be defined over DAGs.

Intuitively, we first observe that deviations from reversibility can be properly captured measuring the uncertainty in reversing a given path, a measure called *topological reversibility* [6]. This measure of uncertainty is provided by the statistical entropy over the set of paths present in a given graph. It turns out that deviations of the pyramidal structure can be also quantified through an information-theoretic measure, namely, from the difference between the amount of statistical entropy generated when we cross the graph according to the flow direction depicted by the arrows and the uncertainty in reversing the paths [6]. The spirit of the measure is to compare the creation of alternatives -new paths- in a top down exploration of the DAG against the irreversibility of these paths. If the quantification of the uncertainty in reversing the paths displays a lower value than the quantification of alternatives, we say that, qualitatively, the net shows a pyramidal structure. If the creation of new paths in a top down exploration of the graph is quantitatively equal to the uncertainty in reversing them, then, there is no argument to attribute to the net any pyramidal shape. Finally if the situation is opposite to the former one, the graph will display a funnel-like or inverted pyramid structure.

The essential point will be thus the computation of the above mentioned uncertainties. The conceptual issue is the following: Let \mathcal{G}_C be the condensed graph of a given graph \mathcal{G} . Since \mathcal{G}_C is a graph without cycles, the set of paths going from M to μ contains a finite number of elements π_1, \dots, π_N . If $v_i \in M$. Therefore, uncertainty associated to follow a given path starting from v_i and ending to some node in μ , $h(v_i)$ will be:

$$h(v_i) = - \sum_{\pi_k \in \Pi_{M\mu}} \mathbb{P}(\pi_k | v_i) \log \mathbb{P}(\pi_k | v_i), \quad [10]$$

where $\mathbb{P}(\pi_k | v_i)$ is the probability that the path π_k is followed, starting from node $v_i \in M$. This entropy was proposed in

[7, 6]. The average uncertainty we face to follow a path starting from some node in M will be

$$H_f(\mathcal{G}_C) = \frac{1}{|M|} \sum_{v_i \in M} h(v_i) \quad [11]$$

which is the general expression of the *forward* entropy of \mathcal{G}_C . The same reasoning can be applied when reversing the flow defined by the arrows in \mathcal{G}_C , thereby obtaining an analogue expression for the *Backwards* entropy of \mathcal{G}_C . However, the direct computation of entropies using equation (10) is extremely difficult and tedious, since the number of paths can combinatorially explode with the size of the graph. Fortunately, we can derive a closed, exact form for such entropies [7, 6].

Backwards entropy

Let \mathcal{G} be a directed graph and \mathcal{G}_C its condensed counterpart. Let $A(\mathcal{G}_C)$ be the adjacency matrix of \mathcal{G}_C . We first define the $|V_C \setminus M| \times |V_C \setminus M|$ matrix $\mathbf{B}(\mathcal{G})$ in the following way:

$$(\forall v_i, v_j : A_{ij} = 1) \quad B(\mathcal{G})_{ij} = \frac{A_{ij}(\mathcal{G}_C)}{k_{in}(v_j)}, \quad [12]$$

and $(\forall v_i, v_j : A_{ij} = 0) \quad B(\mathcal{G})_{ij} = 0$. From this definition, we obtain the explicit dependency of the probability of crossing v_j when we start to reverse a path from v_i , $\mathbb{P}(v_j \leftarrow v_i)$. Thanks to the DAG-like nature of the condensed graph, we can compute such a probability directly from the powers of the adjacency matrix [7], namely,

$$\mathbb{P}(v_j \leftarrow v_i) = \sum_{1 \leq k \leq L(\mathcal{G}_C)} \left([\mathbf{B}^T]^k (\mathcal{G}) \right)_{ij}. \quad [13]$$

Now we compute the average amount of uncertainty we have to face when *reversing* a path. Specifically, we have path starting at some node in M and ending at node $v_j \in \mu$. We want to know the uncertainty of recovering this path if we go

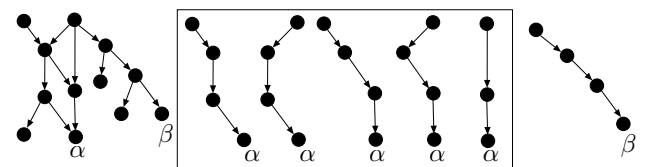


Fig. 9. We have a graph (left). Imagine that we know that some causal chain ended in node α . We have 5 different paths (center, inside the rectangle) to reach α from the top -the maximal nodes. So there is *uncertainty in reversing the path*. Finally (right), we observe that there is no uncertainty in reversing the causal path that ended in β , since there is only one path to go to β from the maximal nodes. In this graph $H_b > 0$ due to the uncertainty arisen when reversing the paths that ended in α .

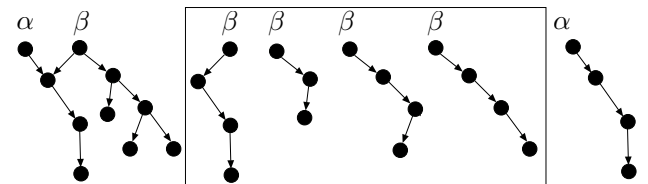


Fig. 10. We have a graph (left). Imagine that we know that some causal chain begun in node β . We have 4 different paths (center, inside the rectangle) to reach a node belonging to the set of minimal nodes. So there is *uncertainty in following the path*. Finally (right), we observe that there is no uncertainty in following the causal path that begun in α , since there is only one path to go from α to the minimal nodes. In this graph, $H_f > 0$, due to the uncertainty arisen in following the paths starting in β .

backwards, i.e., from the node $v_j \in \mu$ to a given node in M . This average uncertainty is provided by the following entropic functional [6]:

$$H_b(\mathcal{G}_C) = \frac{1}{|\mu|} \sum_{v_i \in \mu} \sum_{v_k \in V_C \setminus M} \mathbb{P}(v_i \leftarrow v_k) \cdot \log k_{in}(v_k). \quad [14]$$

Forward entropy

Now we compute the forward version of the above defined entropy. In this case, we need to compute the probability to cross node v_k departing from $v_i \in M$ according to the causal flow -not reversing it, as above. The explicit expression of this probability is defined from matrix $\mathbf{B}'(\mathcal{G})$:

$$(\forall v_i, v_j : A_{ij} = 1) \quad B'(\mathcal{G})_{ij} = \frac{A_{ij}(\mathcal{G}_C)}{k_{out}(v_i)},$$

and $(\forall v_i, v_j : A_{ij} = 1), B'(\mathcal{G})_{ij} = 0$. Then, in analogy to what we found above -equation (13)-, we have that the probability to cross node v_j if we started a path in v_i is

$$\mathbb{P}(v_i \rightarrow v_j) = \sum_{1 \leq k \leq L(\mathcal{G}_C)} \left([\mathbf{B}']^k (\mathcal{G}) \right)_{ij}. \quad [15]$$

The average of the amount of uncertainty emerging when we want to follow a path from which we know that starts in a given $v_i \in M$ and ends in a given node of μ will now be [6]:

$$H_f(\mathcal{G}_C) = \frac{1}{|M|} \sum_{v_i \in M} \sum_{v_k \in V \setminus \mu} \mathbb{P}(v_i \rightarrow v_k) \cdot \log k_{out}(v_k), \quad [16]$$

where M is the set of maximal nodes.

Treeness

The presented coordinate compares the creation of new paths following the causal flow defined by the arrows against the uncertainty to reverse them. The creation of new paths is due to the existence of more than a single alternative to leave a given node. If we create new paths we are thus creating information -quantified by H_f . However, such information can be destroyed by the uncertainty in reversing the paths -evaluated by H_b . Intuitively, a graph having pyramidal structure will have the balance $H_f - H_b$ positive, whereas a graph having inverted pyramidal structure will display $H_f - H_b$ negative. A completely random DAG displays $H_f - H_b \approx 0$ [6]. It turns out that, properly manipulated, such information measures are the perfect indicators of the pyramidal properties of the graph, a key ingredient of our hierarchy coordinates.

In order to generate a normalized estimator (between -1 and 1) accounting for the balance between $H_f(\mathcal{G}_C)$ and $H_b(\mathcal{G}_C)$ we define $f(\mathcal{G})$ as follows:

$$f(\mathcal{G}) \equiv \frac{H_f(\mathcal{G}_C) - H_b(\mathcal{G}_C)}{\max\{H_f(\mathcal{G}_C), H_b(\mathcal{G}_C)\}}. \quad [17]$$

The *treeness coordinate* of a DAG, to be indicated as $T(\mathcal{G})$, will be the average among the $L(\mathcal{G}_C) - 1$ subgraphs $\mathcal{G}_1, \dots, \mathcal{G}_k, \dots, \mathcal{G}_{L(\mathcal{G}_C)-1}$, the $L(\mathcal{G}_C) - 1$ subgraphs $\tilde{\mathcal{G}}_1, \dots, \tilde{\mathcal{G}}_k, \dots, \tilde{\mathcal{G}}_{L(\mathcal{G}_C)-1}$ and \mathcal{G} itself, i.e., the set $\mathcal{W}(\mathcal{G})$ defined in equation (7)⁷, i.e.:

$$\begin{aligned} T(\mathcal{G}) &= \frac{1}{2L(\mathcal{G}_C) - 1} \left(f(\mathcal{G}) + \sum_{i < L(\mathcal{G}_C)} f(\mathcal{G}_i) + f(\tilde{\mathcal{G}}_i) \right) \\ &= \frac{1}{|\mathcal{W}(\mathcal{G})|} \sum_{\mathcal{G}_i \in \mathcal{W}(\mathcal{G})} f(\mathcal{G}_i) \\ &= \langle f \rangle_{\mathcal{W}(\mathcal{G})}, \end{aligned} \quad [18]$$

where $\mathcal{W}(\mathcal{G})$ is the set of subgraphs of \mathcal{G}_C obtained through the application of a lead removal algorithm (either bottom up or top down) and which contain at least one link, as defined in equation (7).

For the sake of consistency we explicitly define the behavior of some limit, potentially problematic cases. When obtaining the sequence of \mathcal{G} 's and $\tilde{\mathcal{G}}$'s the graph can break into more than a single connected component. Let $\Gamma(\mathcal{G}_i) = \{\gamma_1, \dots, \gamma_k\}$ the set of components of our graph \mathcal{G}_i , let $V^i(\gamma_j)$ be the set of nodes of the j -th component of \mathcal{G}_i and let $\tilde{V}^i(\gamma_j)$ the set of nodes of the j -th component of $\tilde{\mathcal{G}}_i$. The parameter $f(\mathcal{G}_i)$ is evaluated averaging the individual contributions of the different connected components of \mathcal{G}_i or $\tilde{\mathcal{G}}_i$ according to the number of nodes they have against $|V_i|$ or $|\tilde{V}_i|$, the set of all nodes of \mathcal{G}_i and $\tilde{\mathcal{G}}_i$, respectively, leading to:

$$\begin{aligned} f(\mathcal{G}_i) &\equiv \frac{1}{|V_i|} \sum_{\Gamma(\mathcal{G}_i)} |V^i(\gamma_k)| f(\gamma_k) \text{ and} \\ f(\tilde{\mathcal{G}}_i) &\equiv \frac{1}{|\tilde{V}_i|} \sum_{\Gamma(\tilde{\mathcal{G}}_i)} |\tilde{V}^i(\gamma_k)| f(\gamma_k). \end{aligned}$$

We impose, for both mathematical and conceptual consistency, that:

$$(\max\{H_b(\mathcal{G}_C), H_f(\mathcal{G}_C)\} = 0) \Rightarrow (T(\mathcal{G}) \equiv 0).$$

Furthermore, if $E_C = \emptyset$, (i.e., the case where the graph consists of a single node):

$$T(\mathcal{G}) \equiv 0.$$

The coordinates of hierarchy for directed graphs. These three coordinates enabled us to define a morphospace, Ω , in which every net will be represented by a point $\mathbf{u}(\mathcal{G}) = (T(\mathcal{G}), F(\mathcal{G}), O(\mathcal{G}))$ in this space. The coordinates defining such space are thought of to grasp the essentials of *hierarchy*,

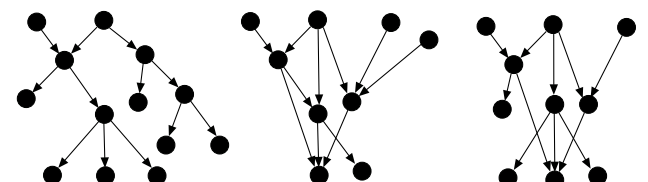


Fig. 11. Gaining intuition: Why do H_b and H_f grasp the hierarchical nature of graphs. The graph on the left displays $H_f - H_b > 0$ and it is thereby hierarchical. On the contrary, the graph on the center displays $H_f - H_b < 0$, being thus anti-hierarchical. Finally, on the right we have a graph such that $H_f - H_b \approx 0$, thus it is neither hierarchical nor anti-hierarchical.

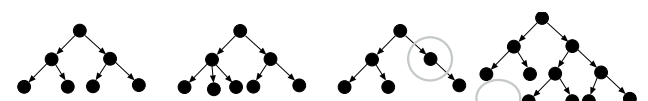


Fig. 12. The need for detailed layer analysis. All four graphs display $H_f > 0$ and $H_b = 0$. However, the two graphs on the right contains a violation on the hierarchy assumptions, namely, the need for *pyramidal* structure at all levels. The dissection allows to identify and penalize such deviations.

⁷Note that i) we ruled out the contributions of $\mathcal{G}_{L(\mathcal{G}_C)}$ and $\tilde{\mathcal{G}}_{L(\mathcal{G}_C)}$ because they contain no links by definition, and, therefore, would impact to the computation of the hierarchy without justification, and ii) consistently, we compute the average between $2L(\mathcal{G}_C) - 1$ objects, the size of the set $\mathcal{W}(\mathcal{G})$ defined in equation (7).

taking as the canonical hierarchical structure the one satisfying the postulates presented in section *Postulates of Hierarchy*. Additionally, as we have seen, comparison between coordinates also provides us valuable information concerning the whole structural organization of the net. For example, the relation between O and F enables us to estimate how many cyclic regions are in the graph and at what point of the causal flow they are located. In addition, they provide an estimator of relevance of coordinate T , since low values of O, F indicate us that the net is mainly cyclical and that the feed-forward-like analysis provided by T is less relevant than in the case where O, F are close to 1. To test the consistency of this coordinate system, we will rigorously check the behavior in several extreme and paradigmatic cases:

Lemma: \mathcal{G} displays $T(\mathcal{G}) = F(\mathcal{G}) = O(\mathcal{G}) = 1$ if and only if \mathcal{G} is a directed tree in which all the leafs have the same length, as defined in section *Directed Graphs*.

Proof

(\Rightarrow) By definition, this graph is a *DAG*, therefore, $F(\mathcal{G}) = O(\mathcal{G}) = 1$. Furthermore, all its nodes but the one in M have $k_{in} = 1$, which means that

$$(\forall \mathcal{G}' \in \{\mathcal{G}_1, \dots, \mathcal{G}_{L(\mathcal{G}_C)-1}\} \bigcup \{\tilde{\mathcal{G}}_1, \dots, \tilde{\mathcal{G}}_{L(\mathcal{G}_C)-1}\})(H_b(\mathcal{G}') = 0). \quad [19]$$

And, since all but the set of minimal nodes will display $k_{out} \geq 2$, then:

$$(\forall \mathcal{G}' \in \{\mathcal{G}_1, \dots, \mathcal{G}_{L(\mathcal{G}_C)-1}\} \bigcup \{\tilde{\mathcal{G}}_1, \dots, \tilde{\mathcal{G}}_{L(\mathcal{G}_C)-1}\})(H_f(\mathcal{G}') > 0), \quad [20]$$

and, thus, $(\max\{H_f(\mathcal{G}'), H_b(\mathcal{G}')\} = H_f(\mathcal{G}'))$

$$(\max\{H_f(\mathcal{G}'), H_b(\mathcal{G}')\} = H_f(\mathcal{G}')).$$

The above claims are also true for the whole graph \mathcal{G} . Therefore, all the $2L(\mathcal{G}_C) - 1$ quotients of the type shown in equation (17) involved in the computation of $T(\mathcal{G})$ will have a value equal to 1, which leads to $T(\mathcal{G}) = 1$.

(\Leftarrow) If $F(\mathcal{G}) = O(\mathcal{G}) = 1$, then \mathcal{G} is a *DAG*. To see that $T(\mathcal{G}) = 1$, it is enough to realize that the graph must satisfy equations (19, 20) and that this can only happen if \mathcal{G} is a directed tree in which all the leaves have the same length. We observe that, if the leaves have not the same length, then a 0 will emerge in some computation, lowering the value to $T(\mathcal{G}) < 1$.

Corollary: \mathcal{G} displays $T(\mathcal{G}) = -1, F(\mathcal{G}) = O(\mathcal{G}) = 1$ if and only if \mathcal{G} is a directed tree in which all the leaves have the same

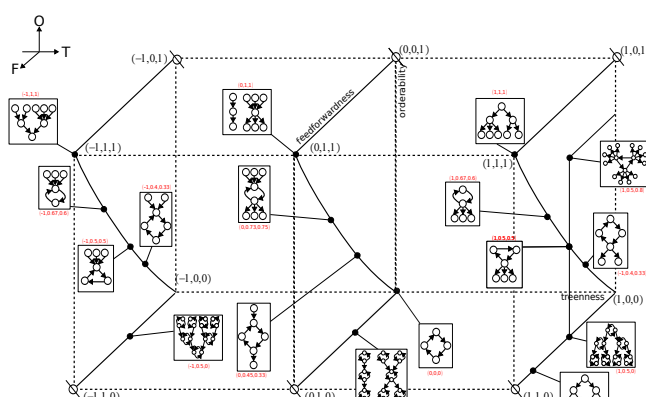


Fig. 13. Illustration of the kind of graphs living in the morphospace Ω . We located different kinds of toy graphs in their corresponding *TFO* coordinates, \mathbf{u} , to grasp the kind of structures one might expect to observe in the different regions of the morphospace. Numbers in red indicate \mathbf{u} for every graph.

length, as defined in section *Directed Graphs* but with changing the direction of all arrows.

This latter case would belong to the perfect *anti-hierarchical* system. A graph consisting in a big cycle will be the paradigmatic example of *non-hierarchical* system, showing thus $T(\mathcal{G}) = F(\mathcal{G}) = O(\mathcal{G}) = 0$. Finally, a graph consisting of a chain of nodes, or a *DAG* in which all the layers have the same size and all nodes the same connectivity will be the paradigmatic example of *non-hierarchical* but *ordered system*, showing $T(\mathcal{G}) = 0, F(\mathcal{G}) = O(\mathcal{G}) = 1$. An illustration of the gallery of conformation on the region of possible networks in the Ω space is provided in figure (13). Notice that some regions of the morphospace cannot be occupied by the very definition of the measures, while others represent strange configurations. It is worth to note that it is mathematically possible to apply this formalism to networks containing more than one connected component. However, meaningful information can only be obtained from the study of a single component since it represents a unique causal structure.

In figure (14) we detail the computation of the hierarchy coordinates of a given graph. From the original directed graph, the process of strongly connected component (*SCC*) detection and condensation give rise a node-weighted con-

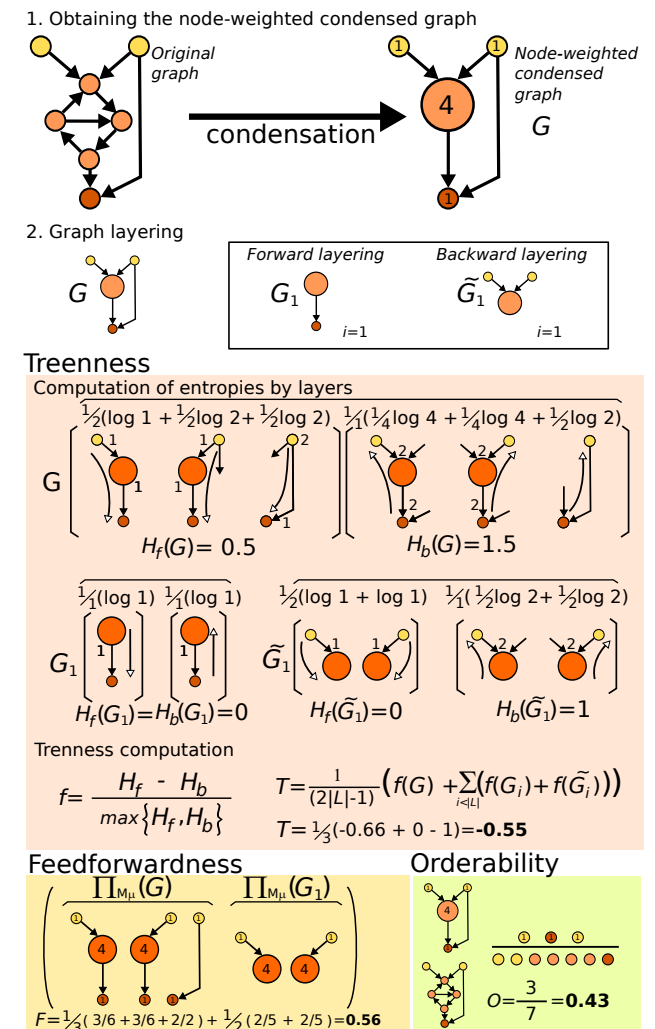


Fig. 14. The definition of the hierarchy-based morphospace Ω . Visual representation of the computation of the three axes of the morphospace: treeness, feedforwardness and orderability (*TFO* coordinates, \mathbf{u}).

densed graph by from the original graph. From this graph, the three coordinates are computed.

Analytical estimates for random graphs. We will now provide estimations for the hierarchy coordinates in random directed graphs. A word of caution is needed. Exact calculations of the above presented values are hard and far away from the scope of this work. We therefore will present the analytic results starting from some simplifying assumptions to obtain indications on what we should expect in the case of large, sparse random networks. We will focus on T and O , since the active presence of paths and cycles in the computation of F makes any rough estimation extraordinarily complex and of no practical use.

T in random directed graphs

We are going to show that the expected value $\langle T \rangle$ over an ensemble of random directed graphs is 0. The reasoning takes advantage of the internal symmetries of the ensemble and uses several critical assumptions which will be clearly highlighted. A totally rigorous derivation of this result would require a deep exploration of such assumptions, something that goes far from the main scope of the presented work.

Let us suppose that we have an undirected graph \mathcal{G} having adjacency matrix $A(\mathcal{G})$. Now, *every undirected link* is transformed into a directed one and the direction of the arrow is defined at random with probability $p = 1/2$. Let us define $G_d(\mathcal{G})$ as the ensemble of all M possible directed graphs we can build from \mathcal{G} by imposing a direction at random over the links present in such graph:

$$G_d(\mathcal{G}) = \{\mathcal{G}_1^d, \dots, \mathcal{G}_M^d\}.$$

Let now A_1^d, \dots, A_M^d be their respective adjacency matrices. In addition, let $(\mathcal{G}_i^d)^T$ be the graph described by the transpose of the adjacency matrix of \mathcal{G}_i^d , $(A_i^d)^T$. We observe that, since directions have been assigned at random:

$$(\mathcal{G}_i^d \in G_d(\mathcal{G})) \Rightarrow \left((\mathcal{G}_i^d)^T \in G_d(\mathcal{G}) \right).$$

For any graph we can build, a graph with all the directions of the links switched can also be built up. We can therefore induce a partition in $G_d(\mathcal{G})$, $\tilde{G}_d(\mathcal{G})$, made of pairs of graphs of $G_d(\mathcal{G})$, namely:

$$\tilde{G}_d(\mathcal{G}) = \{\{\mathcal{G}_1^d, (\mathcal{G}_1^d)^T\}, \dots, \{\mathcal{G}_m^d, (\mathcal{G}_m^d)^T\}\}, \quad [21]$$

and, since this is a partition of $G_d(\mathcal{G})$, we highlight that

$$(\forall x, y \in \tilde{G}_d(\mathcal{G})) (x \cap y = 0) ; \quad \bigcup \tilde{G}_d(\mathcal{G}) = G_d(\mathcal{G}); \quad m = \frac{M}{2}.$$

These properties will be useful in the forthcoming derivations. We observe that the partition of the ensemble in pairs of graphs whose adjacency matrices are mutually transposed will also be possible after the condensation operation, therefore, if $G_c(\mathcal{G})$ is the ensemble of all possible condensed graphs out of all directed graphs composing $G_d(\mathcal{G})$:

$$G_c(\mathcal{G}) = \{\mathcal{G}_1^c, \dots, \mathcal{G}_{M'}^c\},$$

(notice that $M' < M$ in most cases), then,

$$(\mathcal{G}_i^c \in G_c(\mathcal{G})) \Rightarrow \left((\mathcal{G}_i^c)^T \in G_c(\mathcal{G}) \right), \quad [22]$$

also holds. This symmetry within the ensemble $G_c(\mathcal{G})$ is found as long as $p = 1/2$, i.e., directions of links are totally imposed at random. We keep this in mind and we proceed to compute the expected value of the backwards and forward entropy over the ensemble, $\langle H_f \rangle, \langle H_b \rangle$, and we see that:

$$\begin{aligned} \langle H_f \rangle &= \frac{1}{|G_c(\mathcal{G})|} \left[\sum_{\mathcal{G}_\ell^c \in G_c(\mathcal{G})} \right. \\ &\quad \left. \frac{1}{|M_\ell|} \sum_{v_i \in M_\ell} \sum_{v_k \in V \setminus \mu_\ell} \mathbb{P}(v_i \rightarrow v_k) \cdot \log k_{out}(v_k) \right] \\ &= \frac{1}{|G_c(\mathcal{G})|} \left[\sum_{\mathcal{G}_\ell^c \in G_c(\mathcal{G})} \right. \\ &\quad \left. \frac{1}{|M_\ell|} \sum_{v_i \in \mu_\ell} \sum_{v_k \in V \setminus M_\ell} \mathbb{P}(v_i \leftarrow v_k) \cdot \log k_{in}(v_k) \right] \\ &= \langle H_b \rangle, \end{aligned}$$

where M_ℓ and μ_ℓ stand for the maximal and minimal sets of \mathcal{G}_ℓ^c . Notice that the crucial step is the second equality, where we use the symmetry of $G_c(\mathcal{G})$ described in equation (22). We therefore have that

$$\langle H_f \rangle = \langle H_b \rangle.$$

This tells us that $\langle H_f \rangle - \langle H_b \rangle = 0$. However, we cannot jump directly to conclude that $\langle H_f - H_b \rangle = 0$. Using the same reasoning we used above, we compute $\langle H_f - H_b \rangle$:

$$\begin{aligned} \langle H_f - H_b \rangle &= \frac{1}{|G_c(\mathcal{G})|} \sum_{\mathcal{G}_i^c \in G_c(\mathcal{G})} H_f(\mathcal{G}_i^c) - H_b(\mathcal{G}_i^c) \\ &= \frac{1}{|G_c(\mathcal{G})|} \sum_{\{\mathcal{G}_i^c, (\mathcal{G}_i^c)^T\} \in \tilde{G}_c(\mathcal{G})} H_f(\mathcal{G}_i^c) - H_b((\mathcal{G}_i^c)^T) \\ &= 0. \end{aligned}$$

Again, in the second step, we rearranged the terms of the sum by means of the partition $\tilde{G}_c(\mathcal{G})$ -see equation (21)- induced

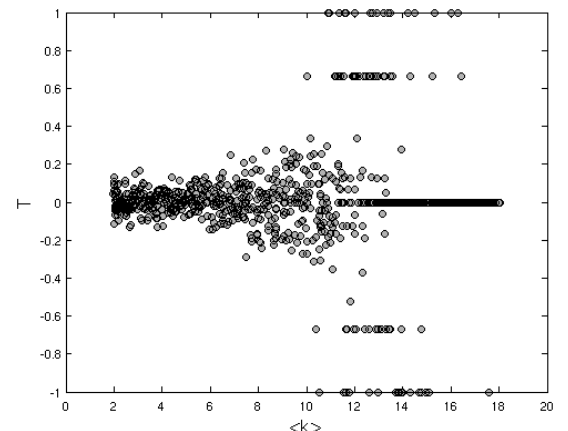


Fig. 15. Evolution of the coordinate T in an ensemble of directed random graphs of size $n = 1000$ in terms of the average degree $\langle k \rangle$. As predicted by equation (23), values accumulate around $T = 0$. As the connectivity increases, the variance increases as well. This is due to the process of condensation, that reduces drastically the size of the graph, since most nodes belong -as we shall see in the next section- to a single cycle. Therefore, the resulting condensed graph is very small and even being maximals directly connected to minimals, thereby revealing, in some cases, extreme values of T , like -1 or 1 .

over the ensemble $G_c(\mathcal{G})$, thereby resetting all terms of the sum to zero. Thus, we can conclude that:

$$\begin{aligned}\langle f \rangle &= \left\langle \frac{H_f - H_b}{\max\{H_f, H_b\}} \right\rangle \\ &= 0.\end{aligned}$$

And, since it is true *in general*, we have proven that given a graph \mathcal{G} , if we build an ensemble of random directed graphs $G_d(\mathcal{G})$ using the procedure described at the beginning of the section, then:

$$\langle T \rangle = 0. \quad [23]$$

A couple of remarks are in force. *i)* The first one concerns the assumption that the ensemble $G_c(\mathcal{G})$ is *well behaved*, which means that the averages collapse to the most probable value of a given observable. As we shall see, this assumption holds in general in ensembles of random graphs, and it seems reasonable to assume that this is independent of the degree distribution, as long as the graph is obtained using the random procedure presented above. *ii)* The second remark concerns cycles containing 2 nodes which, by construction, are avoided in the above developments. However, we observe that these bidirectional links already introduce a symmetry within the adjacency matrix under the transpose operation and, consequently, their presence would have no impact in equation (22) and thus the reasoning still holds. We remark that this is what is observed in random graphs, independently of their degree distributions, as we see in figure (15) and in the forthcoming sections.

O in random directed graphs

Now we will obtain an estimate of the evolution of the O coordinate. To this end we will use standard theory of generating functions applied to the emergence of giant components within a random graph. We will not develop the reasoning since this is far from the scope of the work and they it is clearly developed in [8], [9] or [10]. We recommend the interested reader to go to this literature and references therein.

Let us work with an ensemble of directed random graphs, $\mathcal{G}(V, E)$. The undirected average degree will be thus:

$$\langle k \rangle = \frac{2|E|}{|V|}$$

and the average *in* and *out* degree will be

$$\langle k_{in} \rangle = \frac{|E|}{|V|} = \langle k_{out} \rangle$$

i.e., since directions are spread at random, we assume that $\langle k_{in} \rangle = \langle k_{out} \rangle \approx \frac{\langle k \rangle}{2}$. It is well known that, in general, after a certain threshold of $\langle k \rangle$ the *Giant Connected Component* (*GCC*) emerges, namely, a connected component of \mathcal{G} containing a finite fraction, S , of the nodes of the graph [9]. For directed graphs, in addition, we observe further the emergence of the *Giant Strongly Connected Component*, (*GSCC*) namely, a single *SCC*-see equation (2)- containing a finite fraction \mathbf{S} of the nodes of the graph [8]. The *GSCC* will represent the largest *cyclic region* of the graph. Consequently, if we assume that small *SCCs* that can be also present within the graph represent a negligible fraction of it when compared to the size of the *GSCC*, one can approach the following:

$$O \approx 1 - \frac{\mathbf{S}}{S}. \quad [24]$$

The $1/S$ term acts as a normalization factor over the connected fraction of the graph, since our hierarchy computations only make sense over fully connected structures. Notice that

the probability to have 2 *GCC* is vanishingly small [10] and thus, with high probability

$$GSCC \subset GCC,$$

therefore, the normalization of the relative size of the *GSCC* with the size of the *GCC* provides us an estimation about the actual impact of cycles over the connected structure of the graph. We then use generating function methodology to obtain an estimate both S and \mathbf{S} . Let $f(r)$ be the generating function of the degree distribution, $p(k)$, of the graph \mathcal{G} having average degree $\langle k \rangle$:

$$f(r) = \sum_k p(k)r^k.$$

Then, following [9], we have that

$$S = 1 - f(r_c), \quad [25]$$

being r_c the smallest positive solution of

$$r_c = \frac{1}{\langle k \rangle} \frac{\partial}{\partial r} f(r) \Big|_{r=r_c}.$$

To obtain \mathbf{S} of the random directed graph, one proceeds in an analogous way: Let now $g(x, y)$ be the generating function of the joint *in-degree* and *out-degree* distribution, $p(k_{in}, k_{out})$ of a given random graph \mathcal{G} :

$$g(x, y) = \sum_{k_{in}, k_{out}} p(k_{in}, k_{out}) x^{k_{in}} y^{k_{out}}.$$

Following [8], we know that, if there is no correlation between *in* and *out-degrees* $p(k_{in}, k_{out}) \approx p(k_{in})p(k_{out})$, we can estimate the size of the *GSCC* as:

$$\mathbf{S} = (1 - g(x_c, 1))(1 - g(1, y_c)), \quad [26]$$

where x_c is smallest positive root of the following self-consistent equation:

$$x_c = \frac{1}{\langle k_{in} \rangle} \frac{\partial}{\partial y} g(x, y) \Big|_{x=x_c, y=1},$$

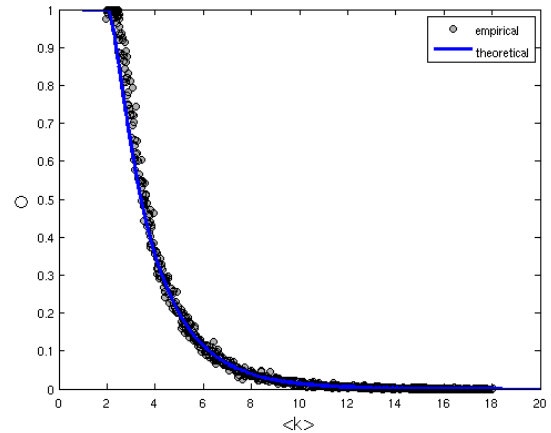


Fig. 16. Evolution of the coordinate O in an ensemble of directed random graphs of $|V| = 1,000$ in terms of the average degree $\langle k \rangle$. Similar behaviour was obtained for ensembles of 500 nodes. The blue line contains the theoretical prediction provided by equation (27) and dots represent actual graphs of the ensemble. As we can see the fitting between real data and the theoretical prediction is, in spite the assumptions made, very good.

and, identically, y_c is smallest positive root of the following self-consistent equation:

$$y_c = \frac{1}{\langle k_{out} \rangle} \frac{\partial}{\partial x} g(x, y) \Big|_{x=1, y=y_c}.$$

We emphasize that this independence condition among k_{in} and k_{out} is a very strong one, consequently, results must be seen as a rough estimation of the qualitative behavior of the GSAC.

To obtain concrete results, we now turn to an ensemble of directed ER graphs with uncorrelated *in* and *out* degrees. In this ensemble, $|E|$ directed links are spread at random among pairs of the $|V|$ existing nodes. The *in* and *out* average degrees will be $\langle k_{in} \rangle = \langle k_{out} \rangle \approx \frac{\langle k \rangle}{2}$, and the degree distribution of the *in* and *out* binomial distribution around the above mentioned averages. Under this framework, one has that:

$$g(x, 1) = e^{\frac{\langle k \rangle}{2}(x-1)}; \quad g(1, y) = e^{\frac{\langle k \rangle}{2}(y-1)};$$

and

$$f(r) = e^{\langle k \rangle(r-1)}.$$

Thereby obtaining an interesting simplification of our problem, namely,

$$\frac{1}{\langle k_{in} \rangle} \frac{\partial}{\partial y} g(x, y) = g(x, y) = \frac{1}{\langle k_{out} \rangle} \frac{\partial}{\partial x} g(x, y).$$

Thus, the above critical values read:

$$x_c = e^{\frac{\langle k \rangle}{2}(x_c-1)} = y_c,$$

and, from equation (24),

$$O = 1 - \frac{(1 - x_c)^2}{1 - r_c}, \quad [27]$$

since, from equation (25) $S = 1 - r_c$.

In figure (16) we plot estimates of equation (27) and real values from an ensemble of Erdos-Renyi graph and we see that, despite the strong assumptions made, the behavior of O can be clearly predicted from the mentioned equation, providing a good insight to the behavior of such coordinate.

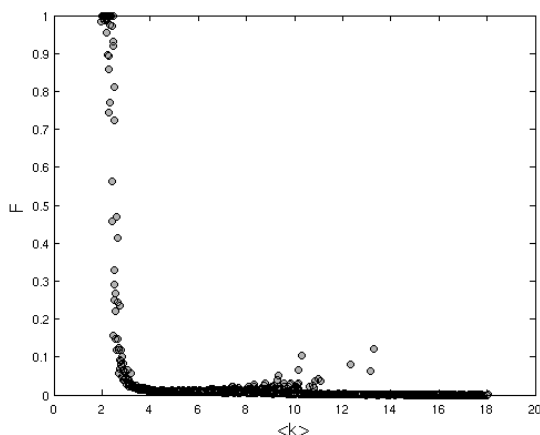


Fig. 17. Evolution of the coordinate F in an ensemble of directed random graphs of $|V| = 1,000$ in terms of the average degree $\langle k \rangle$. Similar behaviour was obtained for ensembles of 500 nodes. Note the slight data dispersion at high $\langle k \rangle$ values. This region correspond to connectivities where the resulting condensed graph is very little. In such circumstance, variations in the position of the SCC in node weighted condensed graph has a considerable impact of F computation.

F in random directed graphs

In order to get insight about the behaviour of this coordinate we provide a numerical computation of F for an ensemble of increasing directed ER networks. Figure (17) shows the dramatic impact of $\langle k \rangle$ in F . In this case, due to F intrinsically depends on the diameter of the graph in the computation of the number of pathways from minimal to maximals in the condensed graph. It is not ignored by the authors that the drastic reduction of F by increasing $\langle k \rangle$ is tied to the impact of SCC size affecting to the length of pathways in the condensed graph. However, we consider that to find this connection go beyond the aim of a work that pursue the presentation of a formalisation and characterization of the concept of hierarchy in the framework of a morphospace. Further work in this direction will contribute to the analytical comprehension of the impact of $\langle k \rangle$ in F .

All the theoretical work is thus finished. From now on, we will apply such machinery to the analysis of both model and real networks.

Analysis of Networks

In this section we systematically study the location of both real and model networks in the morphospace defined by the three coordinates $T(\mathcal{G}), F(\mathcal{G}), O(\mathcal{G})$. We begin by studying classical models of random graphs, namely, the Erdős-Rényi (ER) [11], the Barabási-Albert preferential attachment (BA) [12] and the Callaway-Hopcroft-Kleinberg-Newman-Strogatz uniform attachment (Callaway) [13]. Then, we evaluate the hierarchy coordinates of 125 real networks belonging to different systems. The analysis of real nets is completed by confronting the obtained results with the exploration of the hierarchy coordinates of their corresponding randomized ensembles. We use two randomization methods which are exposed in detail. Finally we present an *in silico* experiment of evolution of networks inside the morphospace. Such analysis enables us to explore the accessibility of the space of possible configurations and sheds light on what is likely to observe in real systems. To end with, we show several figures of real networks before and after the condensation operation, and its intuitive *icon* that enables us to informally describe the general behavior of the causal flow defined by the given net.

Model Networks. Analysis of model networks obtained using the directed versions of ER, BA and Callaway models show similar results. In all cases, model networks having high connectivities aggregate around the region defined by the rectangle $T = (-1, 1), F \approx (0, 0.5), O \approx 0$. The high variance on the value of T can be explained by the fact that \mathcal{G}_c is very small, since high connectivity produces a drastic process of condensation. It is easy to see that a network with a

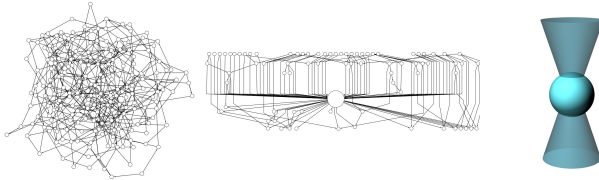


Fig. 18. A representative graph generated through the mechanism of uniform attachment of the ensemble having $\langle k \rangle = 4$ and $|V| = 200$. The original network (left), the giant component of its the condensed version (center) and the illustrative picture according fig. (1) of the main text. The hierarchy coordinates (T, F, O) of this net are $\mathbf{u}(\mathcal{G}) = (-0.09, 0.04, 0.44)$.

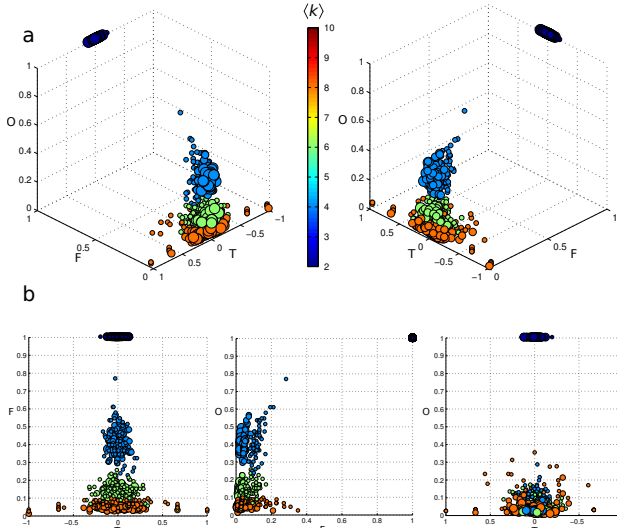


Fig. 19. TFO coordinates, \mathbf{u} , for the Callaway model ensemble. Two views of the Ω 3D representation (a). Projections of the morphospace Ω (b).

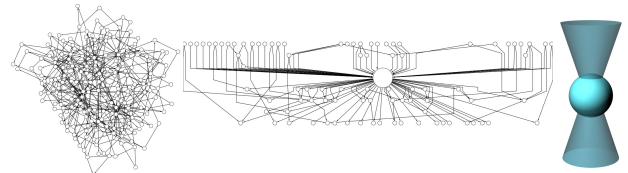


Fig. 20. The giant component of a graph generated through the mechanism of preferential attachment (BA) of the ensemble having $\langle k \rangle = 4$ and $|V| = 200$. The original network (left), the giant component of its the condensed version (center) and the illustrative picture according fig. (1) of the main text. The hierarchy coordinates (T, F, O) of this net are $\mathbf{u}(\mathcal{G}) = (-0.01, 0.07, 0.4)$.

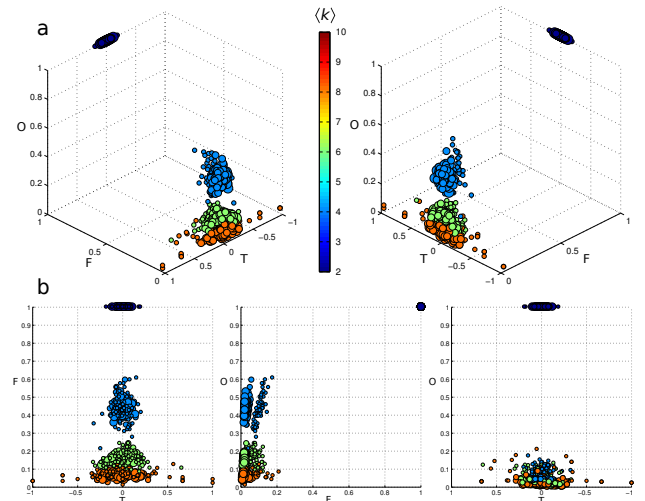


Fig. 21. TFO coordinates, \mathbf{u} , for the BA model ensemble. Two views of the Ω 3D representation (a). Projections of the morphospace Ω (b).

handful of nodes is more likely to give extreme values than large networks. Departing from the value $O \approx 0$ displayed at high connectivities, as connectivity decreases, O starts to increase but nets still aggregate around $T \approx 0$ and $F \approx 0$. For low connectivities, T values tend to be closer to $T = 0$ but both F and O change their behavior, increasing their values to reach the region around the point $T = 0, F = 1, O = 1$. This latter situation can be explained by the low presence -or complete absence- of cycles in networks having small connectivities. Actually, the region $T = 0, F = 1, O = 1$ is only occupied by DAGs.

Below we proceed to detail the exact parameters of the numerical experiments.

Directed ER graphs

We begin with the nets generated by the directed version of the Erdős Rényi model. Such a model consists of two parameters, $|V|$ and p , that specify the size of the network ($|V|$) and the probability of connecting any pair by an arc in any direction (p). For $|V| \gg 0$, this model does not ensure connectedness until values of $p \approx \log(|V|)/|V|$ [14]. An ensemble of 35,760 graphs with three sizes ($|V| = \{100, 250, 500\}$) was created following the following procedure: We create 64 replicas for every graph size starting from $p_{max} = 0.1$. We repeated this process reducing p in a step size of 0.0005 until a value of p able to produce graphs with a fraction of vertices belonging to the giant connected component larger than 97.5%. The resulting ensemble encompasses a range of $100 < \langle k \rangle < 2.51$. See results in figure (23).

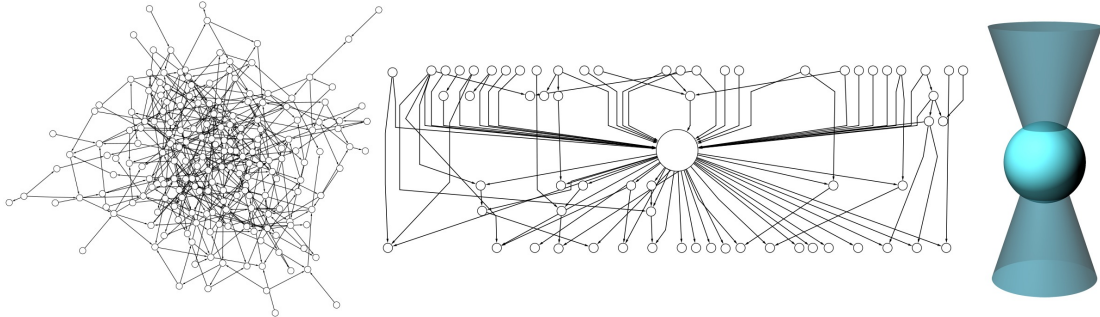


Fig. 22. The giant component of an Erdős-Rényi graph of the ensemble having $\langle k \rangle = 4$ and $|V| = 200$. The original network (left), the giant component of its the condensed version (center) and the illustrative picture according fig. (1) of the main text. The hierarchy coordinates (T, F, O) of this net are $\mathbf{u}(\mathcal{G}) = (0.04, 0.05, 0.33)$.

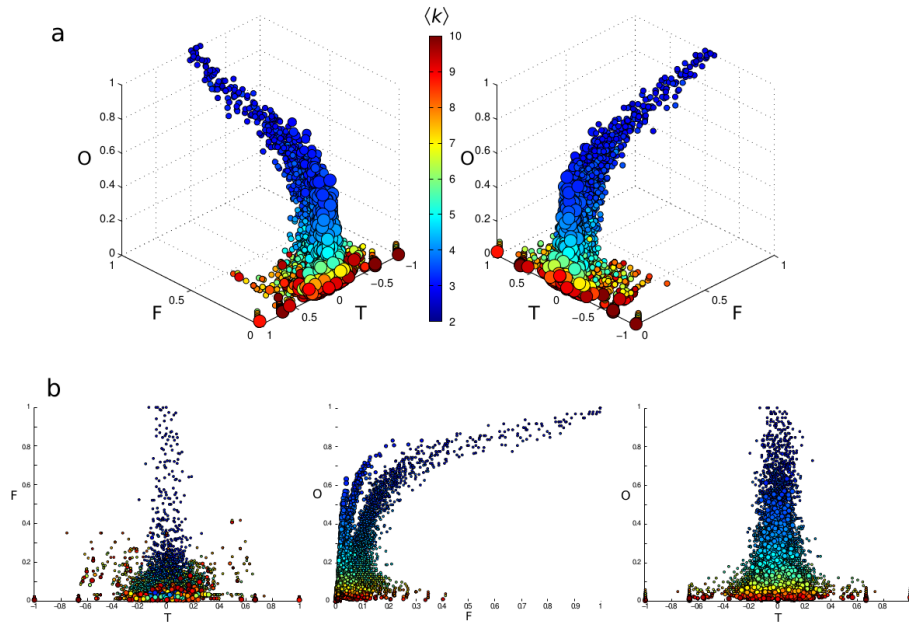


Fig. 23. TFO coordinates for the Erdős-Rényi model ensemble. Two views of the Ω space 3D representation (a). Projections of the morphospace Ω (b).

Directed Callaway graphs

The uniform attachment [13] is an iterative model consisting of three parameters, namely m_0 , m and i . Starting on a fully connected set of m_0 nodes, during i iterations a new node is added to the network. Such node is linked to m existing nodes. These nodes can be selected with equal probability, i.e. there is a *uniform* attachment. Once the iterative process is finished, a random uniform orientation that converts links into directed arcs is performed in order to obtain a directed graph. An ensemble of 768 directed graphs was generated considering 64 replicas of networks for three different sizes($|V| = \{100, 250, 500\}$) and four averages degrees ($\langle k \rangle = \{2, 4, 6, 8\}$). Average degrees correspond with $m = \{1, 2, 3, 4\}$; in each case, the seed is a clique of $m_0 = m$ nodes. See figure (19) for results.

Directed BA graphs

The preferential attachment [12] is an iterative model consisting of three parameters, namely m_0 , m and i . Starting on a fully connected set of m_0 nodes, during i iterations a new node is added to the network. Such node is linked to m of the existing nodes. These nodes are subject to be selected with a prob-

ability proportional to their degree, i.e. there is a preferential attachment. Once the iterative process is finished, a random uniform orientation that converts links into directed arcs is performed in order to obtain a directed graph. An ensemble of 768 directed graphs containing 64 replicas of networks for three different sizes($|V| = \{100, 250, 500\}$) and four averages degrees ($\langle k \rangle = \{2, 4, 6, 8\}$, corresponding to $m = \{1, 2, 3, 4\}$) was generated. See figure (21) for results. As above, the seed is a clique of $m_0 = m$ nodes in all cases.

Real Networks. After looking at the properties of standard models of random networks, we explored a collection of 125 networks encompassing 13 types of systems obtained from real data. Figure (24) shows the resulting TFO morphospace for the real networks used in this work. To discuss the relevance of the observed results, we confronted data of real networks against the one obtained from their randomized counterparts. Randomized ensembles were built using two different techniques of randomization. Below methods and results are detailed, after the network data set presentation.

Network dataset

C elegans cell lineage network. Label: Cellular in the Fig 2 of the article. Cell lineage network obtained from Worm database and published as analysed in [15].

C elegans neural network. Label: Neuronal in the Fig 2 of the article. A directed, weighted network representing the neural network of *C. elegans*. Data compiled by D. Watts and S. Strogatz and made available at the Mark Newman's website: <http://www-personal.umich.edu/mejn/netdata/> used in [16]. Original experimental data taken from [17].

Metabolic networks. Label: Metabolisms in the Fig 2 of the article. Metabolic network set is a selection of 19 reaction-metabolite directed networks obtained from three different published papers for different organisms:

Barabasi dataset for *E.coli*, *B. subtilis*, *S cerevisiae*. <http://www.nd.edu/~networks/resources/metabolic/index.html> from data used in [18].

Networks obtained from the database published in [19]. A selection of 5 multicellular animals: *H. sapiens* (hsa), *M. musculus* (mmu), *D. melanogaster* (dme), *R. norvegicus* (rno) and *C. elegans* (cel). One multicellular plant: *A. thaliana* (ath). Two unicellular fungi: *S. cerevisiae* (sce), *S. pombe* (spo). And seven prokaryotes: *P. Aeruginosa* (pae), *E. coli* (eco), *B. subtilis* (bsu), *Mycoplasma genitalis* (mge), *Mycoplasma pneumoniae* (mpn), *Synechocystis sp.* PCC6803 (syn) and *Salmonella typhimurium* (sty).

The Edinburgh human metabolic network taken from [20].

Food Webs. Label: Food webs in the Fig 2 of the article. These networks describes the exchange flow from the donor to recipient compartments where not necessarily nodes represent single species. The food web set contains a set of 22 directed weighted graphs in their original format. In this article were taken as unweighted directed graphs. Food-webs were originally selected from the R.E. Ulanowicz's Collection from the Ecosystem Network Analysis site and from ATLSS - Network Analysis of Trophic Dynamics in South Florida Ecosystems and compiled in the Pajek dataset. Source: <http://vlado.fmf.uni-lj.si/pub/networks/data/bio/foodweb/foodweb.htm>.

Gene regulatory networks (GRNs) and one kinase network. Label: GRNs and Kinase network respectively, in the Fig 2 of the article. GRNs set contains the networks from two different articles. The data consists of directed networks where nodes are genes and arcs between two genes captures the interaction of the respective gene product -represented by the source node- over the regulatory region of the target gene -target node. The only one available kinase network at the present is represented by a directed network where nodes are proteins and arcs represents the relation of phosphorylation of a protein -node source- over the a target protein -node target. GRNs of *S cerevisiae*, *E. coli*, *Mus musculus*, *Ratus norvegicus*, *Homo sapiens* and *Mycoplasma tuberculosis* and one kinase network of *S cerevisiae* were taken from <http://info.gersteinlab.org/Hierarchy> and published in [21]. GRNs of *S cerevisiae*, *E. coli*, and *Bacillus subtilis* taken from [5].

Electronic circuits. Label: Electronic circuits in the Fig 2 of the article. Directed networks of 50 electronic wiring compiled from ISCAS'89 and ITC'99 sets. Data from electronic circuits used in [22].

Word corpora. Label: Word corpora in the Fig 2 of the article. Four directed lexical graph from different texts according the description in [23]: "Angie's Wren Xmas Tale" (Paul Auster), "Frankenstein or the modern prometeous" (Mary Shelley), "Ulysses" (James Joyce), "Moby dick" (Herman Melville), "Black cat" (Edgar Allan Poe) and a fragment of the New York Times column.

Scientific citation network. Label: Citations in the Fig 2 of the article. A directed and feedforward graph of citations networks. Nodes are articles and every article points to the articles in which it is cited. Papers that cite S. Milgram's 1967 Psychology Today paper or use Small World. Taken from pajek dataset: <http://vlado.fmf.uni-lj.si/pub/networks/data/>

Software networks or dependence networks. Label: Software in the Fig 2 of the article. Ten directed networks capturing the map of file dependencies in different software. In these networks every node is a file. If a file A is called from another file B, then B receives an arrow from A. Although is generally avoided in programming, one file can contain more than one function -argument- and therefore it can be called for more than one purposes. This feature would explain the appearance of cycles in some circumstances. Eight networks were taken from [24]. Two additional networks were obtained from the Internet: r package dependencies: taken from <http://csgillespie.wordpress.com/2011/03/23/graphical-display-of-r-packages-dependencies/> Java packages taken from: <http://gd2006.org/contest/details.php#java>

Ownership:EVAownership. Label: Ownership in the Fig 2 of the article. EVA is a multidisciplinary research project combining information extraction, information visualization, and social network analysis techniques to bring greater transparency to the public disclosure of inter-relationships between corporations. This data corresponds with an ownership network with 6,726 relationships among 8,343 companies. <http://denali.berkeley.edu/eva/> Data obtained form pajek database: <http://vlado.fmf.uni-lj.si/pub/networks/data/econ/Eva.htm> K. Norlen, G. Lucas, M. Gebbie, and J. Chuang. EVA: Extraction, Visualization and Analysis of the Telecommunications and Media Ownership Network. Proceedings of International Telecommunications Society 14th Biennial Conference (ITS2002), Seoul Korea, August 2002.

Blogspol. Label: Social in the Fig 2 of the article. A directed network of hyperlinks between weblogs on US politics, recorded in [25]. Data obtained from pajek database. Original data was taken by pajek database from the Mark Newman's dataset <http://www-personal.umich.edu/mejn/netdata/>

Hitech. Label: Social in the Fig 2 of the article. The case is a small hi-tech computer firm which sells, installs, and maintains computer systems. The network contains the friendship ties among the employees, which were gathered by means of the question: Who do you consider to be a personal friend? A friendship choice (arc) is only included in the network if both persons involved acknowledge it. Taken from <http://vlado.fmf.uni-lj.si/pub/networks/data/esna/hiTech.htm>, published in [26].

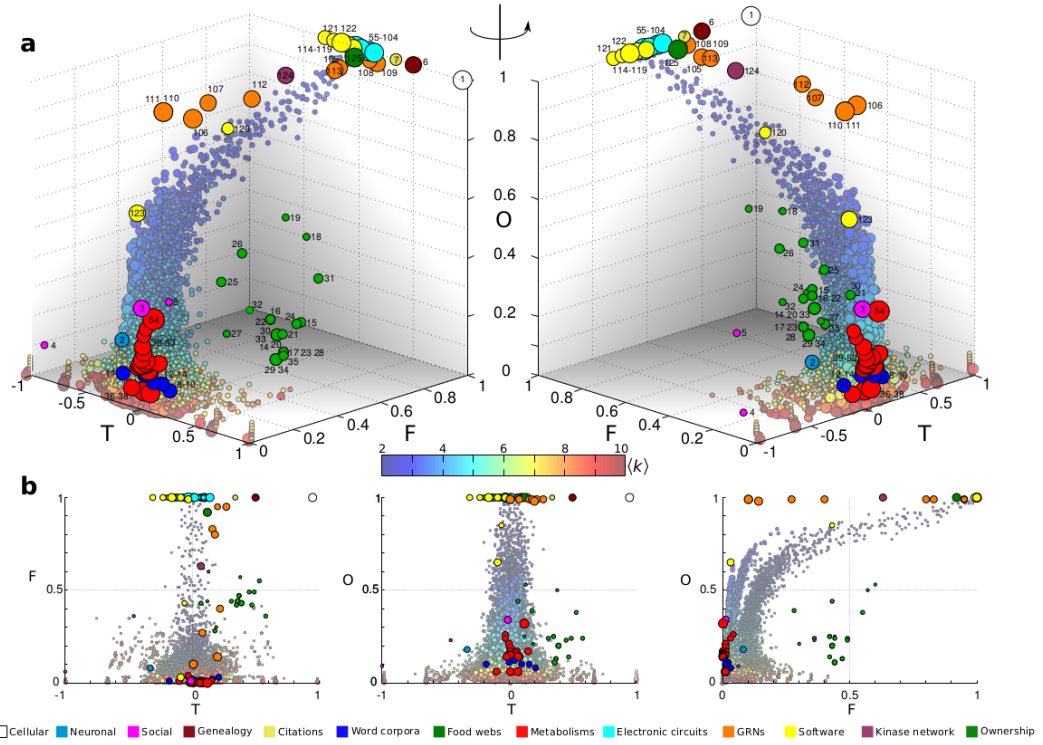


Fig. 24. TFO coordinates, \mathbf{u} , for the real networks studied in this work. Two views of the Ω 3D representation (a). Projections of the morphospace Ω (b). As a transparent layer ER ensembles are superposed.

ModMath. Label: Social in the Fig 2 of the article. Taken from Pajek dataset <http://vlado.fmf.uni-lj.si/pub/networks/data/esna/modMath.htm>. This network concerns the diffusion of a new mathematic method in the 1950s. This innovation was instigated by top mathematicians and sponsored by the National Science Foundation of the USA as well as the U.S. Department of Education. R.O. Carlson, Adoption of Educational Innovations (Eugene: University of Oregon, Center for the Advanced Study of Educational Administration, 1965, p. 19).

PhD advisors (genealogy). Label: Genealogies in the Fig 2 of the article. Data taken from: <http://vlado.fmf.uni-lj.si/~pub/networks/data/esna/CSPhD.htm>. The network contains the ties between Ph.D. students and their advisors in theoretical computer science; each arc points from a supervisor to a student. The partition contains the (estimated) year in which the Ph.D. was obtained. Original author: David Johnson; maintained by Ian Parberry. The SIGACT Theoretical Computer Science Genealogy, Last Updated July 22, 1996. Data taken as appeared in [15].

Randomization Methods

Method A: Preserving the undirected degree sequence and the component structure. In this randomization technique, we generate the ensemble of randomized graphs by taking as topological invariants the undirected degree sequence and the component structure. It is worth to note that the component structure is not preserved using a standard method of graph randomization under the so-called *configuration model* approach [9].

Given an undirected graph $\mathcal{G}(V, E)$, $|V| = n$, its *undirected degree sequence*, $\sigma_u(\mathcal{G})$, is the sequence of n integer numbers

in which the i -th number depicts the undirected degree of node v_i , $k(v_i)$ in a given labelling v_1, \dots, v_n of the nodes of the graph:

$$\sigma_u(\mathcal{G}) = k(v_1), \dots, k(v_i), \dots, k(v_n).$$

Let us suppose that such a graph has a given component structure $\Gamma(\mathcal{G}) = \gamma_1, \dots, \gamma_j$. The randomization method applied here keeps invariant both $\sigma_u(\mathcal{G})$ and $\Gamma(\mathcal{G})$. This is performed using a *directed* version of the *local swap* algorithm [27, 15]. *Local swap* diverges from standard random rewiring algorithms because it keeps invariant the component structure of the graph. The figure below shows how we generate the randomized elements of the ensemble. Let \mathcal{G} be a directed graph. We choose three links such that they form a chain of length three in \mathcal{G}_u , figure (25, left), i.e., a " \square " structure, no matter the direction of the arrows. Then, we cross the links at the extremes of the chain, i.e., generating a " \times " structure, figure (25 center). Finally, we flip the senses of the arrows at random and, thus, links a and b have transformed into a' and b' . If a' or b' previously existed, we abort this randomizing event and we restart looking at random for another \square structure within the graph.

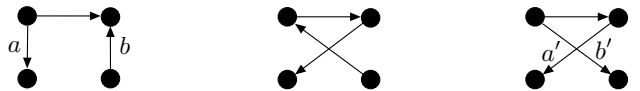


Fig. 25. A local swap algorithm keeping the undirected degree sequence invariant.

For every real network we generated an ensemble of 100 replicas obtained after applying the randomization algorithm until we performed $4|E|$ link switches or $20|E|$ trials. The latter applies generally if the net belongs to an ensemble having a few members, which can happen due to several reasons,

mainly, if the net is too dense or if the net is very sparse, or if it has a non-standard component structure. Numerical details of the randomization process for each real network are described in figs. (44) and (45).

Method B: Preserving the directed degree sequence and the component structure. Now we generate the ensemble of randomized graphs by taking as topological invariants the directed degree sequence and the component structure. Given a directed graph $\mathcal{G}(V, E)$, $|V| = n$, its *directed degree sequence*, $\sigma(\mathcal{G})$, is the sequence of n pairs of integer numbers in which the first number of the i -th pair depicts the *in-degree* of node and the second one depicts the *out-degree* of node v_i , in a given labelling v_1, \dots, v_n of the nodes of the graph:

$$\sigma(\mathcal{G}) = \langle k_{in}(v_1), k_{out}(v_1) \rangle, \dots, \langle k_{in}(v_n), k_{out}(v_n) \rangle.$$

Let us suppose that such a graph has a given component structure $\Gamma(\mathcal{G}) = \gamma_1, \dots, \gamma_j$. The randomization method applied here keeps invariant both $\sigma(\mathcal{G})$ and $\Gamma(\mathcal{G})$. The conservation of $\sigma(\mathcal{G})$ makes this randomization method slightly more restrictive than the other presented above. Specifically, we look for \square structures in \mathcal{G} to perform a *Local Swap*, but, now, the sense of the arrows matter. Indeed, the kind of \square structures over which we can apply a local swap keeping the directed degree sequence of the graph are:

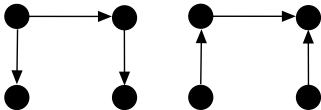


Fig. 26. Structures over which a directed *Local Swap* operation can be applied keeping the directed degree sequence of the graph invariant.

The kind of \square structures over which we cannot apply a directed *Local Swap* operation, if we want to keep the directed degree sequence of the graph invariant are:

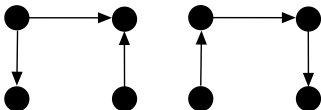


Fig. 27. Structures over which a directed *Local Swap* operation cannot be applied in this case.

Figure (28) shows how we generate the randomized elements of the ensemble. First, we select at random a structure of the kind described in figure (26), figure (28, left). Then, we cross the links at the extremes of the chain, i.e., generating a “ \times ” structure (28 center). Finally, we check if new links a' and b' previously existed. If so, we abort this rewiring event and we restart another one looking at random for structures like the ones described in figure (26).

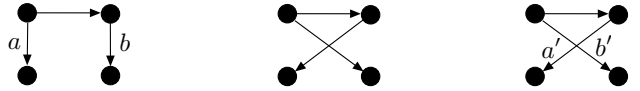


Fig. 28. A local swap algorithm keeping the directed degree sequence invariant.

For every real network we generated an ensemble of 100 replicas obtained after applying the randomization algorithm until we performed $4|E|$ link switches or $20|E|$ trials, if the net belongs to an ensemble having a few members.

Confronting real data with their randomized counterparts

Network randomization offers a quantitative picture of how far real networks are from their respective randomly generated ensembles whose correlations are eliminated by an iterative process of arc rewiring. Comparison is given by contrasting the *TFO* coordinates, \mathbf{u} , of a particular real network with a distribution of values obtained from a randomized ensemble represented by its percentiles in a box plot fashion. This chart allows us to elude any assumption on the statistical behavior of the ensembles of randomized graphs. Figure (29) shows the comparison between real and random ensemble data, the latter generated according methods **a** and **b**. Studied networks appear clustered by types, and every type of network has an associated color. Numbers, network labels, colors and other additional network quantifiers are detailed in figs. (44) and (45). In the figure, real network values are represented in charts by a grey square. The distribution of *TFO* values for every generated ensembles is represented in a box plot. Percentiles 25th, and 75th are represented by an empty blue line box while the percentile 50th is depicted with a red line inside. Whiskers show the values within percentiles 10th and 90th. Finally, red crosses display the values out for the whisker range.

In figure (29) looking at the position of real networks, they fall out from the percentile 50th of their randomized ensembles in the Ω space. Therefore, we can argue that real networks of under scrutiny have not a representative graphical configuration for their degree sequence. This indicates that, although real networks tend to live in the null model regions as we saw earlier, system's constraints confer differences in the pattern of connections that distinguish real networks from their randomized counterparts. This difference is more accentuated for method **a** (the directed degree sequence is not conserved) than for method **b**, mainly due to the fact that the latter imposes a more dramatic restriction in the graphical configuration.

In relation to *T* coordinate, graphs tend to show *T* values close to zero. However, there are exceptions. Positive biased values are observed in food webs and most of GRNs. Such nets are thus hierachic ($T > 0$), in terms of how the causal flow is organized. On the contrary, electronic circuits show an anti hierachical configuration ($T < 0$), with a tendency to occupy slightly negative, but significant, values of *T*. Looking at *F* and *O* values, real networks are generally far from the whiskers of the ensemble, when confronting real data against the ensemble obtained using the randomization method **a** -where directed degree sequence is preserved. In most cases real data appears to avoid the general cyclic character observed in randomized networks. This trend seems to be reduced when the directed degree sequence is conserved (randomization method **b**). This points to the conclusion that not local correlation among connectivities but the pattern of inputs and outputs would explain part of *TFO* values. In general, such a trend presents a larger cyclic character in randomizations than in

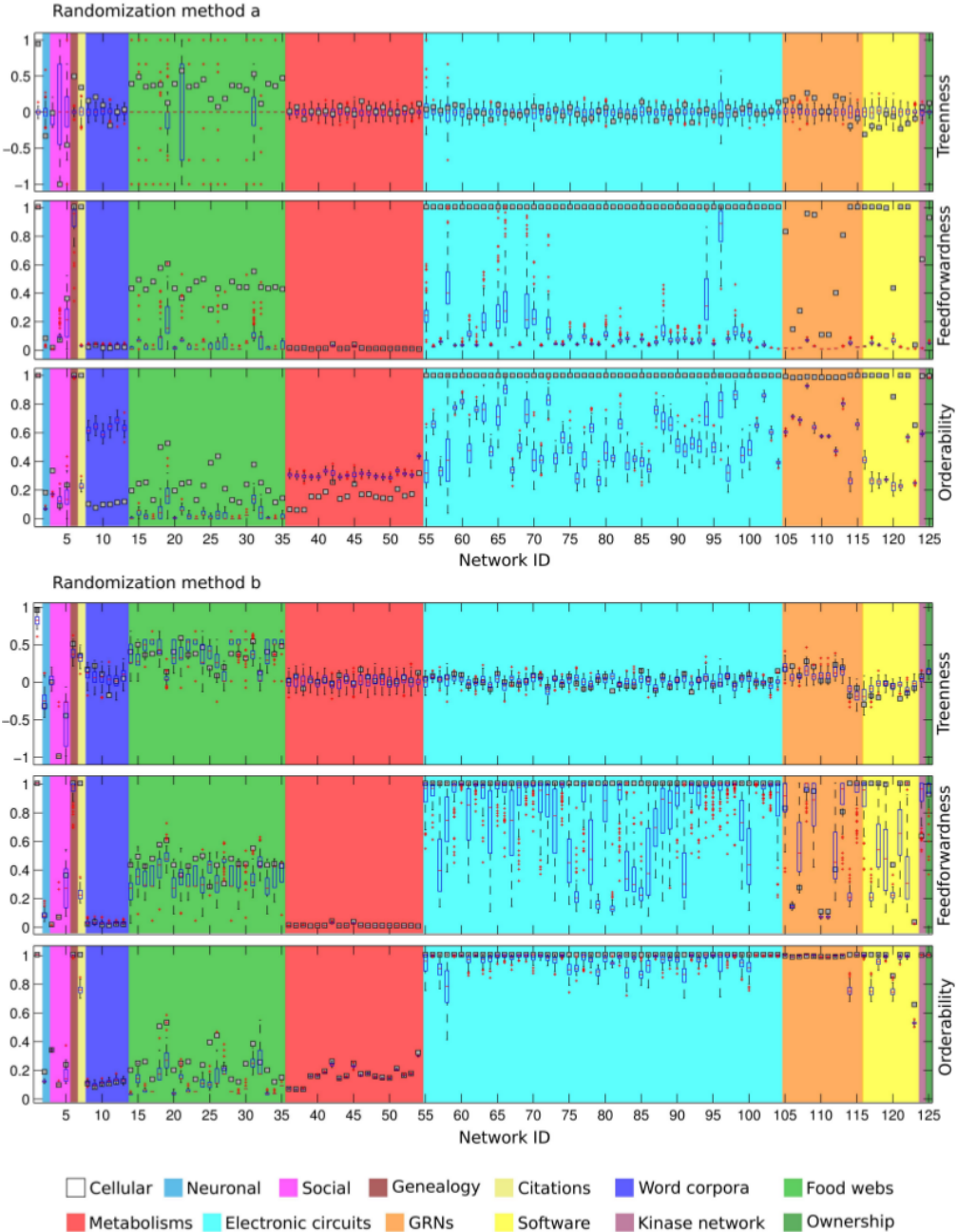


Fig. 29. Comparison of real networks with randomized ensembles according methods **a** (upper part) and **b** (bottom part). In two groups of three charts, the figure displays three box plots for every randomization method showing the comparison of T, F, O values of the real value with its respective randomized ensemble. X axis labels networks ordered by network ID. See Fig. (44) and (45) of this document for ID network information.

real networks. However, we can observe two exceptions to this general behavior. Looking at the O for randomized ensembles obtained through method **a**, metabolisms and word corpora show a higher cyclic character than their respective randomized ensembles. However, when compared to randomized ensembles obtained using method **b**, the trend is similar

to the common values observed in randomized versions. As it happened in the previous cases, the range occupied by real and randomized data seems to be fairly justified in most cases by directed degree sequence.

⁸Given two points $\mathbf{u}_1 = (T_1, F_1, O_1)$, $\mathbf{u}_2 = (T_2, F_2, O_2) \in \Omega$, the distance is computed using the standard euclidean norm, namely:

$$d(\mathbf{u}_1, \mathbf{u}_2) = \sqrt{(T_1 - T_2)^2 + (F_1 - F_2)^2 + (O_1 - O_2)^2}.$$

The accessibility of the Morphospace: Evolution.

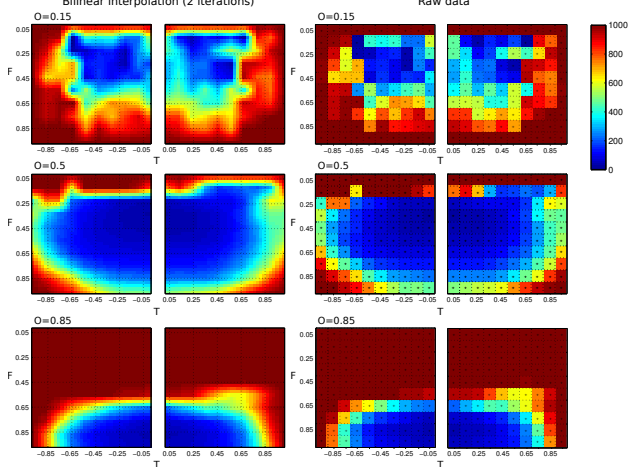


Fig. 32. Accessibility of the morphospace by evolutionary driven network conformation. Three slices of the T-F plane at orderability $O=0.15$ (top), $O=0.5$ (medium), $O=0.85$ (bottom) are presented with a bilinear interpolation (left) and as raw data (right). A scale of false colour represents the number of steps required in an average of 250 replicas by the evolutionary algorithm to achieve a given region of the morphospace.

Now we shall concern ourselves to an *in silico* experiment based on an evolutionary algorithm applied to graph population variation. So far we studied how both real nets and their corresponding random ensembles cover the different regions of the morphospace Ω . The numerical experiment presented below will give us important information on how *accessible* are the different regions of the morphospace if we impose selective pressures related to specific values of hierarchy coordinates over the possible graphs. In raw words, we let evolve a *population* of graphs taking as selective pressure the distance of such graphs to a given target point of Ω . For a given graph, the closer it is to this target point, the higher is its selective value. At the global, evolutionary level, what we want to evaluate is how long it takes to reach a given target point: The more it takes the population to reach it, the more *inaccessible* is this region considered.

Let us detail the experiment. Using a method described in [28] we quantified the accessibility of a grid of points in the defined 3D morphospace Ω . This experiment has a high computational cost, thus, we covered Ω by a grid containing 100 points in three cuts, corresponding to three *TF* planes at three different values of orderability. The three planes are the ones defined by $O = \{0.15, 0.5, 0.85\}$. For each decided O value, along the *TF* plane, minimum and maximum coordinates were distanced a value of 0.05 distance units⁸ from the boundaries and all points of the grid were equally distanced at 0.10. Each of the resulting *TFO* points was used as a target to be reached or approached by a euclidean distance in the 3D morphospace. We say that to *reach* a given target *TFO* point, \mathbf{u}^* , is done when at least one graph of an evolving population acquires a *TFO* value \mathbf{u} such that the euclidean distance between \mathbf{u} and \mathbf{u}^* is smaller than 0.05 distance units. The initial condition of this algorithm is defined by a population of graphs P (always single connected components), being $|P| = 25$, each one made of $|V| = 25$ nodes, generated following the directed Erdős Rényi model with $p = 0.08$ (see section *Model networks* for model details).

At each evolutionary iteration (generation) we perform the following steps:

- Computation of the *TFO* values $\mathbf{u}(\mathcal{G})$ for all $\mathcal{G} \in P$.

- For each graph \mathcal{G} of P , we compute the euclidean distance $d(\mathbf{u}(\mathcal{G}), \mathbf{u}^*)$ between $\mathbf{u}(\mathcal{G})$ and desired target point $\mathbf{u}^* \in \Omega$.
- We calculated the average of the euclidean distance over the population $\langle d(\mathbf{u}(\mathcal{G}), \mathbf{u}^*) \rangle$.
- We applied the selection criterion: we eliminate from the P those graphs satisfying $d(\mathbf{u}(\mathcal{G}), \mathbf{u}^*) > \langle d(\mathbf{u}(\mathcal{G}), \mathbf{u}^*) \rangle$. The set of *survivals* is $P' = \{\mathcal{G} \in P : d(\mathbf{u}(\mathcal{G}), \mathbf{u}^*) \leq \langle d(\mathbf{u}(\mathcal{G}), \mathbf{u}^*) \rangle\}$.
- We create a sequence $\mathbf{s}_{P'}$ picking at random and copying elements from P' . We perform this operation $|P \setminus P'|$ times -therefore, the sequence has length $\ell(\mathbf{s}_{P'}) = |P \setminus P'|$, and repetitions are allowed.
- We apply the *randomization operator* over all graphs of the sequence, keeping the graphs of P' invariant. After this step, together with the unchanged graphs excluded from the rewiring process, we obtaining the new generation of P .

This evolutionary algorithm is then performed a number of 1000 generations. The *randomization operator* is applied to every graph of the sequence $\mathbf{s}_{P'}$ and consists in two steps:

- Random addition from one up to three arcs.
- Random deletion from one up to three arcs of a graph. This step must satisfy the condition of preserving the single connected component. If not, randomization event is aborted and new arcs are chosen to be removed.

There is one situation defined by two conditions for which evolutionary algorithm can be stacked: Given a generation, *i*) if none of the graphs become close enough to the target point and *ii*) none or all graphs are below the fitness mean of the population. Then, to avoid the evolutionary algorithm freezes, the following rule is applied:

- Half of the population is chosen at random to be eliminated and replaced by the other half, giving rise to P' .

For each target point of the grid, 250 replicas of the evolutionary experiment were performed. Each population pursuing a target point was allowed to evolve up to 1000 generations. The average number of generations needed to reach each target point was used as an estimator of the accessibility of that part of Ω . Those cases were the accessibility value is exactly 1000 indicate that none of the graphs in none of the 250 processes was able to reach that target point -see figure (29) for results. In these cases, we expect that more than 1000 generations are needed.

A note of caution must be added to interpret the strength of the obtained results. It is worth to note that parameters of the evolutionary algorithm may be determinant in shaping the observed fitness landscape, thereby accelerating or slowing the convergence process to the desired target point. The aim of this experiment was just to shed light on how accessible different regions of Ω are, considering selection and evolution driving forces. In this context, we numerically answered this question choosing a combination of parameters which we consider to be enough representative to provide us relevant information. And indeed, thanks to this approximation, we showed that not all regions are equally accessible but, instead, some regions are fairly improbable to be achieved. Among other factors, the size of the network may play a crucial role to achieve certain regions of the morphospace, since, for example it is easier for small networks to display extreme configurations.

Both the null model approach and the evolutionary algorithm -as shown in figure (29)- give us clues about the accessibility, either by chance or by driven search, of a particular region of Ω . Both approaches define clearly what we should call the *expected region* -waiting for a better name- in which

almost all null models fall and in which evolution as the driving force seems to successfully push the nets to achieve the target without extreme difficulties. Figures (23,,) and (29) show the kind of network configurations that are likely to be observed -This is the *possible*. The actual distribution of networks within this morphospace is more or less convergent with this *expected region*, although significant deviations can be found, as discussed above. The behavior of real networks and their comparison with real models is shown in figures (24) and (29) -they describe the *actual*.

The described results create a nice, global picture of what is possible and what is actually observed within the zoo of complex networks. This objective is achieved from a rigorous definition of hierarchy.

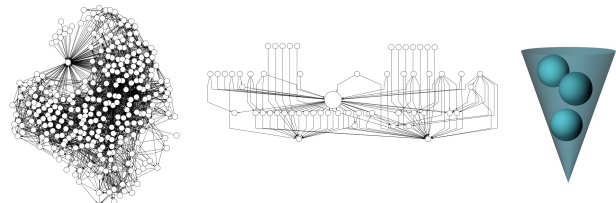


Fig. 31. An example of neural network: The *C. elegans* neuronal wiring data set (net number 2 of SI 2). The original network (left), the giant component of its condensed version (center) and the illustrative picture according fig. (1) of the main text. The hierarchy coordinates (T, F, O) of this net are $\mathbf{u}(\mathcal{G}) = (-0.33, 0.08, 0.18)$

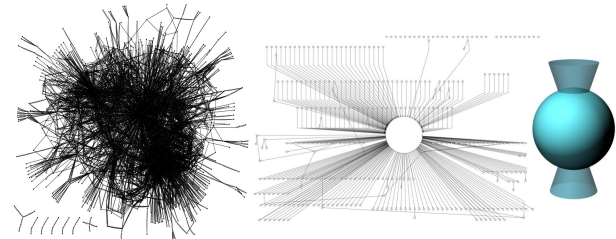


Fig. 33. An example of metabolic network: The Human metabolic network (net number 39 of Fig. 45) data set. The original network (left), the giant component of its condensed version (center) and the illustrative picture according fig. (1) of the main text. The hierarchy coordinates (T, F, O) of this net are $\mathbf{u}(\mathcal{G}) = (0.01, 0.00, 0.15)$.

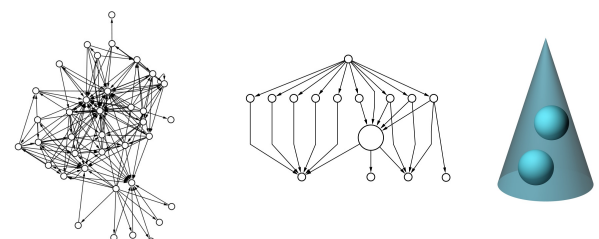


Fig. 34. An example of food-web: The Cheslower (net number 31 of Fig. 44) data set. The original network (left), the giant component of its condensed version (center) and the illustrative picture according fig. (1) of the main text. The hierarchy coordinates (T, F, O) of this net are $\mathbf{u}(\mathcal{G}) = (0.53, 0.55, 0.38)$

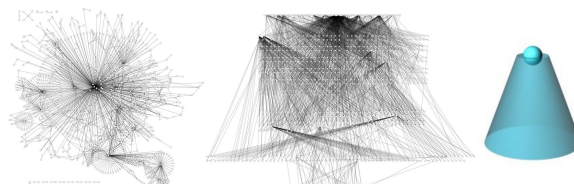


Fig. 35. An example of gene regulatory network: The *B. subtilis* gene regulatory network (net number 113) data set. The original network (left), the giant component of its condensed version (center) and the illustrative picture according fig. (1) of the main text. The hierarchy coordinates (T, F, O) of this net are $\mathbf{u}(\mathcal{G}) = (0.18, 0.8, 0.99)$.

Real Nets Analysis: Figures

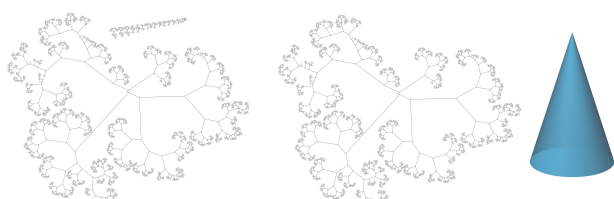


Fig. 30. An example of cell lineage network: The *C. elegans* lineage network (net number 1 of Fig. 45) data set. The original network (left), the giant component of its condensed version (center) and the illustrative picture according fig. (1) of the main text. The hierarchy coordinates (T, F, O) of this net are $\mathbf{u}(\mathcal{G}) = (0.95, 1, 1)$.

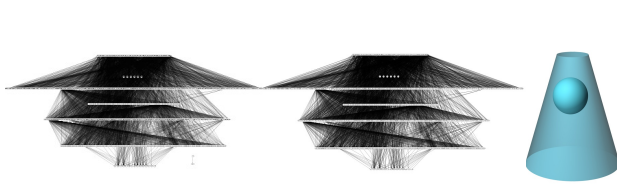


Fig. 36. An example of Kinase network: The yeast protein kinase network (net number 124 of Fig. 44) data set. The original network (left), the giant component of its condensed version (center) and the illustrative picture according fig. (1) of the main text. The hierarchy coordinates (T, F, O) of this net are $\mathbf{u}(\mathcal{G}) = (0.07, 0.63, 0.99)$.

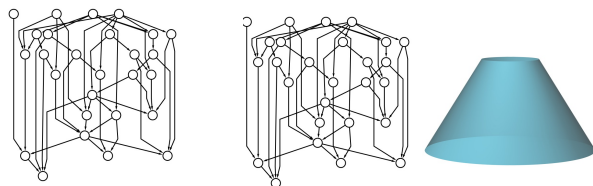


Fig. 37. An example of electronic circuit network: The b03 circuit network (net number 58 of Fig. 44) data set. The original network (left), the giant component of its condensed version (center) and the illustrative picture according fig. (1) of the main text. The hierarchy coordinates (T, F, O) of this net are $\mathbf{u}(\mathcal{G}) = (0.06, 1, 1)$.

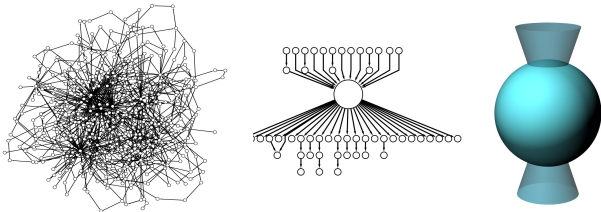


Fig. 38. An example of word corpus network: The NYTIMES.edgl network (net number 12 of Fig. 44) data set. The original network (left), the giant component of its condensed version (center) and the illustrative picture according fig. (1) of the main text. The hierarchy coordinates (T, F, O) of this net are $\mathbf{u}(\mathcal{G}) = (0.00, 0.02, 0.11)$.

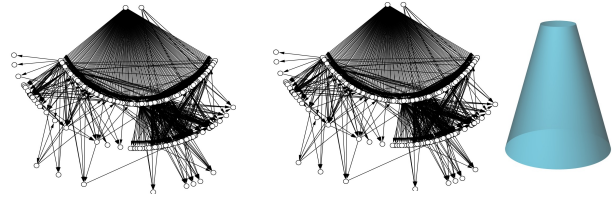


Fig. 39. An example of citation network: The 1967 Milgram's citation network (net number 7 of Fig. 44) data set. The original network (left), the giant component of its condensed version (center) and the illustrative picture according fig. (1) of the main text. The hierarchy coordinates (T, F, O) of this net are $\mathbf{u}(\mathcal{G}) = (0.34, 1, 1)$.

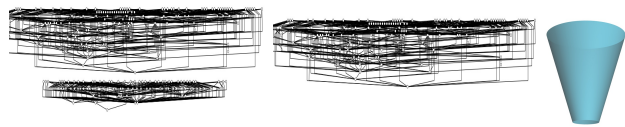


Fig. 40. An example of software network: The dcpp.net network (net number 117 of Fig. 45) data set. The original network (left), the giant component of its condensed version (center) and the illustrative picture according fig. (1) of the main text. The hierarchy coordinates (T, F, O) of this net are $\mathbf{u}(\mathcal{G}) = (-0.19, 1, 1)$.

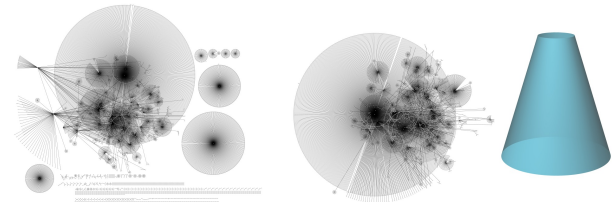


Fig. 41. An example of ownership network: The EVA company ownership network (net number 125 of Fig. 45) data set. The original network (left), the giant component of its condensed version (center) and the illustrative picture according fig. (1) of the main text. The hierarchy coordinates (T, F, O) of this net are $\mathbf{u}(\mathcal{G}) = (0.12, 0.92, 0.99)$.

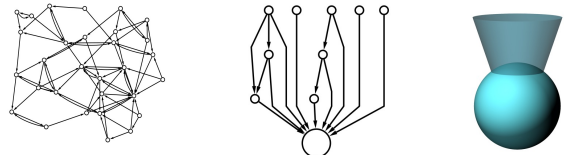


Fig. 42. An example of social network: The ModMath network (net number 5) data set. The original network (left), the giant component of its condensed version (center) and the illustrative picture according fig. (1) of the main text. The hierarchy coordinates (T, F, O) of this net are $\mathbf{u}(\mathcal{G}) = (-0.46, 0.36, 0.23)$.

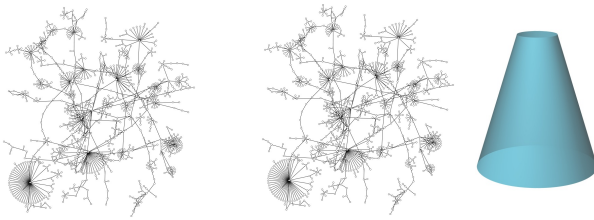


Fig. 43. An example of genealogy network: The PhD advisor's network (net number 6) data set. The original network (left), the giant component of its condensed version (center) and the illustrative picture according fig. (1) of the main text. The hierarchy coordinates (T, F, O) of this net are $\mathbf{u}(\mathcal{G}) = (0.5, 1, 1)$.

Numerical data from real and randomized networks

For that reader interested in numerical details of the set of real networks studied in this work we include a table, divided in figs. 44 and 45, that corresponds with the data obtained from the characterization of the TFO values from the set of real networks. Additional values regarding size of the nets are also provided. Furthermore, the table contains a comparison of TFO real data with the two randomized ensembles described in the section "Randomization methods" of this SI by using a Z-value statistics. Note that for accurate comparison, Z-value approximation assumes that data must follow a normal distribution. However, figure 29 clearly shows that this assumption cannot be ensured for many of the networks analyzed in this study. Limited sizes and extreme degree sequence configurations (such a the tree structure) are strong impositions for randomization methods. By this reason, results of Z-score must be taken with caution, just as an additional evidence of the different deviations of real data from their randomized counterparts.

Net #	Net file	Type	V	E	real data			Z value for randomization type a ensemble						Z value for randomization type b ensemble												
					T	F	O	Z(T)	Z(F)	Z(O)	<T>	s.d.	<F>	s.d.	<O>	s.d.	Z(T)	Z(F)	Z(O)	<T>	s.d.	<F>	s.d.	<O>	s.d.	
1	net1celegans'	celular'	2476	2475	0.95	1	1	23.66	inf	inf	0	0.04	1	0	1	0	1.92	inf	inf	0.81	0.07	1	0	1	0	
2	net10neuronalcelegans'	neuronal'	297	2345	-0.3	0.08	0.2	-2.84	12.93	17.64	0	0.12	0.01	0.01	0.07	0.01	-0.57	0.03	9.36	-0.26	0.12	0.08	0.03	0.12	0.01	
3	net19polblogsCgc'	social'	1222	19021	0	0.01	0.3	0.08	49.89	31.3	-0.02	0.13	0	0	0.17	0.01	-0.25	10.52	0.22	0.01	0.07	0.01	0	0.33	0	
4	net30hiTech'	social'	33	147	-1	0.06	0.1	-1.79	-0.81	-1.11	0.02	0.57	0.11	0.05	0.14	0.04	-0.37	-0.36	-0.37	-0.92	0.23	0.09	0.07	0.09	0.01	
5	net31modMath'	social'	30	76	-0.5	0.36	0.2	-1.17	1.36	0.84	0.03	0.42	0.2	0.12	0.16	0.09	0.06	0.53	1.28	-0.48	0.33	0.28	0.14	0.16	0.06	
6	net32PhD'	genealogy'	1025	1043	0.5	1	1	15.15	0.82	1.49	0	0.03	0.9	0.12	0.98	0	1.54	0.69	1.02	0.37	0.08	0.95	0.07	1	0	
7	net44citations'	citations'	233	994	0.34	1	1	3.04	265.9	35.22	0.01	0.11	0.02	0	0.23	0.02	0.44	18.46	8.36	0.31	0.07	0.23	0.04	0.75	0.03	
8	net52AUSTER'	corpus'	404	759	0.16	0.02	0.1	2.8	-5.85	-17.85	0	0.06	0.03	0	0.62	0.03	0.65	-0.62	-0.31	0.09	0.1	0.02	0.01	0.11	0.01	
9	net53FRANKENS'	corpus'	423	794	0.21	0.03	0.1	3.95	-1.49	-19.62	0	0.05	0.03	0	0.64	0.03	1.52	0.39	-1.61	0.05	0.1	0.02	0.01	0.09	0.01	
10	net54JOYCE'	corpus'	378	734	0.1	0.01	0.1	1.4	-8.15	-17.11	0.01	0.06	0.03	0	0.59	0.03	0.56	-1.42	-1	0.04	0.09	0.02	0.01	0.11	0.01	
11	net55MOBYDICK'	corpus'	442	804	-0.2	0.01	0.1	-3.19	-8.44	-20.07	0.01	0.06	0.03	0	0.64	0.03	-2.57	-1.93	-1.73	0.02	0.08	0.02	0.01	0.12	0.01	
12	net56NYTIMES'	corpus'	473	796	0	0.02	0.1	0.26	-5.11	-21.08	-0.01	0.05	0.04	0	0.69	0.03	0.05	-1	-1.29	0	0.09	0.02	0.01	0.13	0.01	
13	net57POEBLACKCAT'	corpus'	408	752	0.04	0.01	0.1	0.6	-6.13	-17.41	0	0.06	0.03	0	0.63	0.03	-0.42	-0.94	-0.41	0.08	0.1	0.02	0.01	0.12	0.01	
14	baydry.pa[j]	foodweb'	128	2137	0.39	0.43	0.2	2.07	53.19	41.23	-0.02	0.2	0.01	0.01	0	0	0.43	1.67	29.27	0.33	0.14	0.26	0.1	0.03	0.01	
15	ChesMiddle.pa[j]	foodweb'	37	201	0.49	0.49	0.2	0.93	7.81	7.29	0	0.53	0.06	0.05	0.04	0.03	1.82	1.66	2.92	0.29	0.11	0.35	0.08	0.14	0.04	
16	cypdry.pa[j]	foodweb'	71	640	0.35	0.42	0.3	0.68	28.07	16.8	0.08	0.39	0.02	0.01	0.02	0.01	-1.52	1.52	15.16	0.48	0.08	0.33	0.06	0.05	0.01	
17	gramdry.pa[j]	foodweb'	69	910	0.37	0.47	0.1	3.78	51.59	24.93	-0.01	0.1	0	0.01	0	0	-3.55	1.45	7E+014	0.54	0.05	0.32	0.11	0.04	0	
18	Maspalomas.pa[j]	foodweb'	24	82	0.38	0.57	0.5	1.06	4.38	9.7	0.04	0.32	0.09	0.11	0.05	0.05	-0.56	2.12	5.6	0.44	0.1	0.42	0.07	0.18	0.06	
19	Rhode.pa[j]	foodweb'	19	53	0.13	0.6	0.5	0.33	3.4	3.98	-0.01	0.4	0.2	0.12	0.16	0.09	1.83	2.21	2.58	0.03	0.05	0.48	0.05	0.28	0.09	
20	baywet.pa[j]	foodweb'	128	2106	0.39	0.43	0.2	0.11	52.86	45.26	0	0	0.01	0.01	0	0	0.18	1.66	19.62	0.37	0.15	0.28	0.09	0.03	0.01	
21	ChesUpper.pa[j]	foodweb'	37	205	0.58	0.36	0.2	0.79	3.87	7.76	0.07	0.65	0.08	0.07	0.06	0.02	1.62	0.21	2.76	0.36	0.14	0.34	0.08	0.15	0.03	
22	cypwet.pa[j]	foodweb'	71	631	0.35	0.42	0.3	1.05	26.43	17.09	-0.04	0.37	0.02	0.02	0.01	0.01	-1.71	1.66	16.26	0.49	0.08	0.33	0.06	0.05	0.01	
23	gramwet.pa[j]	foodweb'	69	911	0.37	0.47	0.1	Inf	95.22	52.32	0	0	0	0.01	0	0	-2.3	1.46	7E+014	0.53	0.07	0.32	0.11	0.04	0	
24	Michigan.pa[j]	foodweb'	39	218	0.45	0.49	0.2	1.15	13.12	9.26	-0.03	0.42	0.05	0.03	0.03	0.02	0.9	1.95	5.34	0.32	0.15	0.29	0.11	0.02	0	
25	SitMarks.pa[j]	foodweb'	54	353	0.18	0.28	0.4	0.73	13.66	29.13	0	0.25	0.02	0.02	0.01	0.01	-1.71	-1.91	8.9	0.38	0.12	0.41	0.07	0.09	0.03	
26	Chesapeake.pa[j]	foodweb'	39	176	0.07	0.43	0.4	0.29	6.02	14.7	-0.03	0.36	0.05	0.06	0.03	0.03	-1.18	1.27	3.37	0.27	0.17	0.32	0.09	0.15	0.08	
27	CrystalC.pa[j]	foodweb'	24	125	0.19	0.3	0.2	1.14	4.66	7.23	-0.01	0.17	0.04	0.06	0.02	0.03	1.77	-3.75	0.44	0.04	0.09	0.46	0.04	0.19	0.04	
28	Everglades	foodweb'	69	911	0.37	0.47	0.1	Inf	95.22	52.32	0	0	0	0.01	0	0	-2.31	1.47	7E+014	0.53	0.07	0.32	0.1	0.04	0	
29	mangdry.pa[j]	foodweb'	97	1491	0.36	0.44	0.1	Inf	61.01	28.84	0	0	0	0.01	0	0	-1.6	0.96	11.82	0.48	0.07	0.36	0.08	0.03	0.01	
30	Mondego.pa[j]	foodweb'	46	392	0.31	0.44	0.2	1.4	8.09	28.66	0.01	0.21	0.05	0.05	0.02	0.01	-1.71	2.88	14.33	0.52	0.12	0.31	0.05	0.07	0.01	
31	ChesLower.pa[j]	foodweb'	37	165	0.53	0.55	0.4	1.05	8.01	5.85	0.03	0.48	0.11	0.06	0.14	0.04	1.73	3.08	3.29	0.37	0.09	0.33	0.07	0.25	0.04	
32	CrystalD.pa[j]	foodweb'	24	99	0.12	0.44	0.3	0.51	4.24	4.66	-0.03	0.29	0.08	0.08	0.05	0.04	0.52	-0.06	0.07	0.06	0.11	0.44	0.09	0.24	0.11	
33	Florida.pa[j]	foodweb'	128	2106	0.39	0.43	0.2	1.4	52.92	45.27	0	0	0.01	0	0	0	0.19	1.66	19.72	0.37	0.15	0.15	0.28	0.09	0.03	0.01
34	mangwet.pa[j]	foodweb'	97	1492	0.36	0.44	0.1	3.54	52.24	24.9	0.01	0.1	0	0.01	0	0	-1.35	0.97	13.78	0.48	0.09	0.36	0.08	0.03	0.01	
35	Narragan.pa[j]	foodweb'	35	218	0.47	0.42	0.1	Inf	14.68	8.95	0	0	0.02	0.03	0.01	0.01	-0.71	0.59	19.9	0.52	0.07	0.38	0.08	0.09	0	
36	net178SmelCgc'	met	2207	5525	0.01	0.01	0.1	0.22	19.01	-19.6	0	0.05	0	0	0.31	0.01	0.35	5.7	-0.03	-0.01	0.07	0	0	0	0.06	
37	net188CmetCgc'	met	2268	5755	0.07	0.01	0.1	1.68	6.52	-17.66	0	0.04	0	0	0.3	0.01	0.66	3.35	0.96	0.01	0.09	0	0	0.06	0	
38	net20SCmetCgc'	met	1511	3833	-0.1	0.01	0.1	-2.21	5.05	-14.84	0	0.05	0.01	0	0.3	0.02	-1.2	1.69	-0.39	0	0.09	0.01	0	0.06	0	
39	reactions.hsa.txt'	met	2275	6914	0.01	0	0.2	0.17	-4.57	-16.27	0	0.05	0	0	0.29	0.01	-0.12	1.5	0.71	0.02	0.07	0	0	0.15	0	
40	reactions.spo.txt'	met	1386	4181	0	0	0.2	-0.17	-1.53	-12.65	0	0.06	0.01	0	0.29	0.01	0.2	1.52	-0.85	-0.02	0.07	0	0	0.16	0	
41	reactions.ath.txt'	met	1581	4430	0.01	0.01	0.2	0.45	2.29	-11.08	-0.01	0.06	0	0	0.33	0.01	-0.02	5.8	2.77	0.02	0.07	0	0	0.18	0	
42	reactions.mge.txt'	met	337	850	0	0.04	0.3	-0.22	3.72	-2.45	-0.01	0.07	0.02	0	0.32	0.02	0.3	3.17	1.99	-0.05	0.06	0.02	0	0.23	0.01	
43	reactions.stm.txt'	met	1869	5449	0.08	0	0.1	1.33	0.5	-16.07	0.01	0.06	0	0	0.29	0.01	1.29	4.92	1.46	-0.02	0.08	0	0	0.13	0	
44	reactions.bsu.txt'	met	1678	4850	0.03	0.01	0.2	0.68	4.41	-15.4	0	0.05	0	0	0.3	0.01	0.15	7.04	2.83	0.02	0.08	0	0	0.15	0	
45	reactions.mpn.txt'	met	369	957	0	0.03	0.2	-0.29	3.58	-2.72	0	0.08	0.02	0	0.31	0.02	0.21	3.7	1.88	-0.04	0.07	0.02	0	0.22	0.01	
46	reactions.syn.txt'	met	1265	3632	0.15	0.01	0.2	3.01	5.12	-12.14	-0.01	0.05	0.01	0	0.31	0.01	0.18	1.86	7.59	3.38	0.01	0.08	0	0	0.16	0
47	reactions.cel.txt'	met	1480	4293	0.06	0	0.2	0.98	-3.1	-12.53	0	0.06	0	0	0.31	0.01	0.75	0.87	0.02	0	0.08	0	0	0.17	0	
48	reactions.pae.txt'	met</																								

Part 2/2		Net #	Net file	Type	V	E	real data			Z value for randomization type a ensemble						Z value for randomization type b ensemble									
T	F	O	Z(T)	Z(F)	Z(O)	<T>	s.d.	<F>	s.d.	<O>	s.d.	Z(T)	Z(F)	Z(O)	<T>	s.d.	<F>	s.d.	<O>	s.d.					
83	b10.gf3.txt'	circuits'	183	355	-0.1	1	1	-0.73	71.55	7.74	-0.01	0.07	0.08	0.01	0.4	0.08	-1.18	2.72	2.26	0	0.05	0.41	0.22	0.87	0.06
84	s1494.gf3.txt'	circuits'	661	1399	-0.1	1	1	-1.36	569.9	18.19	0	0.05	0.02	0	0.41	0.03	-1.16	4.3	2.47	-0.01	0.05	0.34	0.15	0.97	0.01
85	s386.gf3.txt'	circuits'	172	353	0.14	1	1	1.74	83.67	11.34	0.01	0.08	0.07	0.01	0.39	0.05	1.9	6.38	3.62	0.03	0.06	0.25	0.12	0.86	0.04
86	b11.gf3.txt'	circuits'	475	966	0.04	1	1	0.47	299	17.08	0.01	0.06	0.03	0	0.35	0.04	0.6	1.97	1.62	0	0.07	0.45	0.28	0.92	0.05
87	s1512.gf3.txt'	circuits'	866	1321	-0.1	1	1	-2.34	59.58	6.1	0	0.05	0.05	0.02	0.76	0.04	-0.58	1.81	1.8	-0.09	0.05	0.7	0.17	0.99	0.01
88	s420.gf3.txt'	circuits'	252	399	0.07	1	1	1.13	10.59	3.84	0	0.06	0.15	0.08	0.69	0.08	1.29	0.99	1.22	0.02	0.04	0.8	0.2	0.96	0.03
89	s938.gf3.txt'	circuits'	512	819	-0.1	1	1	-1.38	44.84	5.65	0	0.06	0.06	0.02	0.66	0.06	-1.23	1.04	1.63	-0.03	0.04	0.8	0.2	0.97	0.02
90	b12.gf3.txt'	circuits'	329	586	0.02	1	1	0.24	36.97	6.83	0	0.06	0.07	0.03	0.51	0.07	-0.05	0.95	1.64	0.02	0.06	0.89	0.12	0.96	0.02
91	s444.gf3.txt'	circuits'	205	373	0.1	1	1	1.59	49.52	7.78	0	0.06	0.08	0.02	0.48	0.07	1.37	2.66	2.23	0.03	0.05	0.38	0.23	0.86	0.06
92	s953.gf3.txt'	circuits'	440	772	-0.1	1	1	-2.88	102.7	7.8	0.01	0.05	0.04	0.01	0.53	0.06	-3.46	0.56	0.91	-0.03	0.03	0.95	0.09	0.99	0.01
93	b13.gf3.txt'	circuits'	329	586	0.02	1	1	0.24	36.99	6.85	0	0.06	0.07	0.03	0.51	0.07	-0.04	0.93	1.61	0.02	0.06	0.89	0.12	0.96	0.02
94	s208.gf3.txt'	circuits'	122	189	0.04	1	1	0.37	3.25	2.33	0.01	0.08	0.36	0.2	0.72	0.12	-0.26	0.43	0.77	0.06	0.08	0.97	0.06	0.98	0.02
95	s967.gf3.txt'	circuits'	439	792	-0.1	1	1	-1.12	132.5	9.39	0.01	0.06	0.04	0.01	0.5	0.05	-0.73	0.48	0.87	-0.02	0.05	0.97	0.07	0.99	0.01
96	s27.gf3.txt'	circuits'	17	21	0	1	1	-0.22	1.05	1.35	0.01	0.22	0.84	0.15	0.81	0.14	-0.46	0.54	0.68	0.01	0.12	0.96	0.07	0.94	0.08
97	s499.gf3.txt'	circuits'	175	361	0.07	1	1	0.98	68.58	9.63	-0.01	0.08	0.07	0.01	0.33	0.07	-0.02	0.38	0.59	0.07	0.06	0.97	0.08	0.99	0.02
98	s991.gf3.txt'	circuits'	603	836	0	1	1	-0.87	16.23	3.83	0.01	0.05	0.14	0.05	0.86	0.04	0.65	0.29	0.87	-0.08	0.06	0.98	0.07	1	0.01
99	s298.gf3.txt'	circuits'	136	257	0.05	1	1	0.55	37.28	7.11	0.01	0.08	0.1	0.02	0.44	0.08	0.69	1.45	1.6	0.02	0.05	0.72	0.19	0.94	0.04
100	s510.gf3.txt'	circuits'	236	430	0.09	1	1	1.3	55.08	6.77	0.01	0.06	0.07	0.02	0.49	0.08	1.04	2.03	1.74	0.03	0.06	0.49	0.25	0.91	0.05
101	s669.gf3.txt'	circuits'	3402	5582	0	1	1	-0.41	689.6	17.87	0	0.05	0.01	0	0.65	0.02	-0.88	0.34	1.64	0.01	0.04	1	0.01	1	0
102	s9234.gf3.txt'	circuits'	5787	8129	0	1	1	-0.6	112.9	8.96	0	0.05	0.03	0.01	0.86	0.02	-0.41	1.02	3.61	-0.01	0.04	0.96	0.04	0.99	0
103	s4863.gf3.txt'	circuits'	2495	4196	0.02	1	1	0.71	1175	20.08	-0.01	0.04	0.01	0	0.6	0.02	1.86	0.56	1.44	-0.07	0.05	0.98	0.04	1	0
104	b14.gf3.txt'	circuits'	4721	9775	0.14	1	1	3.85	10074	44.48	0	0.04	0	0	0.39	0.01	4.14	0.76	1.24	-0.01	0.03	0.85	0.21	1	0
105	net45GRN_Gerstein_Ecoli'	GRNs'	1373	2958	0.16	0.83	1	2.53	3181	39.53	0.01	0.06	0.01	0	0.6	0.01	-0.31	-0.26	-2.31	0.19	0.08	0.87	0.15	1	0
106	net46GRN_Gerstein_human'	GRNs'	3101	6878	0.2	0.14	1	3.84	1766	52.73	0.01	0.05	0	0	0.71	0.01	2.88	0.28	-1.01	0.05	0.05	0.14	0.01	0.99	0
107	net47GRN_Gerstein_Mouse'	GRNs'	1185	2389	0.08	0.27	1	1.31	583	28.8	0	0.06	0.01	0	0.69	0.01	0.4	-1.38	-1.72	0.06	0.04	0.56	0.21	0.99	0
108	net48GRN_Gerstein_Mtuberc'	GRNs'	687	828	0.27	0.95	1	3.6	134.7	8.72	0	0.07	0.06	0.01	0.93	0.01	1.48	-0.29	-4.28	0.14	0.08	0.97	0.06	1	0
109	net49GRN_Gerstein_rat'	GRNs'	524	1084	0.2	0.95	1	3.29	639.7	21.89	-0.01	0.06	0.02	0	0.64	0.02	2.37	0.7	-1.37	0.06	0.06	0.82	0.17	0.99	0
110	net50GRN_Gerstein_yeast'	GRNs'	4441	12873	0.01	0.1	1	0.14	2819	75.3	0	0.05	0	0	0.57	0.01	-1.29	4.21	3.59	0.08	0.06	0.07	0.01	0.98	0
111	net5balajibabu'	GRNs'	4441	12873	0.01	0.1	1	0.16	2775	74.47	0	0.05	0	0	0.57	0.01	-1.28	4.19	3.56	0.08	0.06	0.07	0.01	0.98	0
112	net7grnecoli'	GRNs'	1589	4038	0.22	0.4	1	3.77	2592	48.76	0	0.06	0	0	0.47	0.01	1.09	-0.52	-1.86	0.13	0.08	0.51	0.21	0.99	0
113	net16baailus'	GRNs'	892	1327	0.18	0.8	1	3.39	566.9	16.09	0	0.05	0.02	0	0.8	0.01	0.74	-0.69	-3.1	0.13	0.07	0.9	0.14	1	0
114	dcpp_1.net'	software'	132	470	-0.2	1	1	-1.51	76.71	28.8	0	0.13	0.05	0.01	0.26	0.03	-1.3	17.61	6.26	-0.1	0.07	0.21	0.04	0.75	0.04
115	postgresql.net'	software'	779	1446	-0.1	1	1	-1.38	1398	23.89	-0.01	0.06	0.01	0	0.66	0.01	1.18	0.52	0.61	-0.2	0.09	0.95	0.1	1	0
116	xfree150594.net'	software'	393	1104	-0.3	1	1	-3.97	580.4	24.6	0	0.08	0.02	0	0.41	0.02	-1.2	0.76	0.94	-0.19	0.1	0.89	0.14	0.99	0.01
117	dcpp.net'	software'	132	470	-0.2	1	1	-1.47	72.7	28.22	0	0.13	0.05	0.01	0.26	0.03	-1.3	17.57	6.16	-0.1	0.07	0.21	0.04	0.75	0.04
118	tortoisecvs_010605.net'	software'	229	791	-0.2	1	1	-3.22	224.2	30.93	0.02	0.07	0.03	0	0.26	0.02	-3.46	2.2	2.03	-0.03	0.05	0.57	0.19	0.95	0.02
119	xfree86cc.net'	software'	1299	5241	0	0.99	1	-0.35	3506	84.59	0	0.08	0	0	0.27	0.01	0.11	1.98	1.31	-0.03	0.05	0.48	0.26	0.98	0.01
120	emule_i40902.net'	software'	108	349	-0.1	0.43	0.9	-0.56	23.98	17.65	0.01	0.12	0.06	0.02	0.23	0.04	0.16	6.86	3.75	-0.07	0.05	0.22	0.03	0.74	0.03
121	virtualdub_030405.net'	software'	479	1956	-0.2	1	1	-3.05	537	49.06	0	0.08	0.01	0	0.23	0.02	-4.44	1.7	1.68	-0.04	0.04	0.65	0.21	0.98	0.01
122	r_packages'	software'	2425	5358	-0.2	1	1	-3.11	6852	49.74	0	0.05	0	0	0.57	0.01	-0.93	2.74	1.9	-0.11	0.05	0.37	0.23	0.99	0.01
123	net43java'	software'	1538	8032	-0.1	0.03	0.7	-1.4	188.5	58.56	0	0.07	0	0	0.25	0.01	-1.23	9.17	14.62	-0.03	0.05	0.01	0	0.52	0.01
124	net51kinase_Gerstein_yeast'	kinase'	1405	4071	0.07	0.63	1	1.2	2954	46.56	-0.01	0.06	0.01	0	0.59	0.01	0.89	-2.23	-1.7	0.03	0.04	0.91	0.12	1	0
125	net11ownership'	ownership	4475	4662	0.12	0.92	1	3.62	148	7.84	0	0.03	0.04	0.01	0.98	0	-0.29	-0.11	-4.42	0.14	0.05	0.94	0.12	1	0

Legend:

(colors coincide with those used for network type labelling in figures of the article and supplementary information)

|V|: # of nodes

Z(T): Z value for T

<T>: average T of the randomized ensemble

s.d.: standard deviation

|E|: # of arcs

F: feedforwardness

Z(F): Z value for F

<F>: average F of the randomized ensemble

inf: infinite

Fig. 45. Numerical data of the set of real networks (part 2 of 2).

1. Gross J, Yellen J (1998) *Graph Theory and its applications* (CRC, Boca Raton, Florida).
2. Kelley J (1955) *General Topology* (Van Nostrand).
3. Suppes P (1960) *Axiomatic Set Theory* (Dover, New York).
4. Cosentino-Lagomarsino M, Jona P, Bassetti B (2005) Logic backbone of a transcription network. *Phys Rev Lett* 95:158701.
5. Rodríguez-Caso C, Corominas-Murtra B, Solé RV (2009) On the basic computational structure of gene regulatory networks. *Mol Biosyst* 5:1617–29.
6. Corominas-Murtra B, Rodríguez-Caso C, Goñi J, Solé R (2011) Measuring the hierarchy of feedforward networks. *Chaos* (Woodbury, N.Y.) 21:016108.
7. Corominas-Murtra B, Rodríguez-Caso C, I.R. V. Solé JG (2010) Topological reversibility and causality in feed-forward networks. *New J. of Phys.* 12:113051.
8. Dorogovtsev SN, Mendes JFF, Samukhin AN (2001) Giant strongly connected component of directed networks. *Phys. Rev. E* 64:025101.
9. Newman MEJ, Strogatz SH, Watts DJ (2001) Random graphs with arbitrary degree distributions and their applications. *Phys. Rev. E* 64:026118.
10. Newman M (2010) *Networks: An Introduction* (Oxford University Press, Inc., New York, NY, USA).
11. Erdos P, Renyi A (1960) On the evolution of random graphs. *Publ. Math. Inst. Hung. Acad. Sci* 5:17–61.
12. Barabasi AL, Albert R (1999) Emergence of scaling in random networks. *Science* 286:509–512.
13. Callaway DS, Hopcroft JE, Kleinberg JM, Newman MEJ, Strogatz SH (2001) Are randomly grown graphs really random? *Physical Review E* 64:026118+.
14. Bollobás B (1985) *Random Graphs* (Academic Press, London).
15. Goñi J, Corominas-Murtra B, Solé RV, Rodríguez-Caso C (2010) Exploring the randomness of directed acyclic networks. *Phys. Rev. E* 82:066115.
16. Watts DJ, Strogatz SH (1998) Collective dynamics of 'small-world' networks. *Nature* 393:440–442.
17. White JG, Southgate E, Thompson N, Brenner S (1986) The structure of the nervous system of the nematode *caenorhabditis elegans*. *Phil. Trans. R. Soc. London* 314:1–340.
18. Jeong H, Tombor B, Albert R, Oltvai ZN, Barabsi AL (2000) The large-scale organization of metabolic networks. *Nature* 407:651–654.
19. Ma H, Zeng AP (2003) Reconstruction of metabolic networks from genome data and analysis of their global structure for various organisms. *Bioinformatics* 19:270–277.
20. Ma H, et al. (2007) The edinburgh human metabolic network reconstruction and its functional analysis. *Mol Syst Biol* 3:135.
21. Bhardwaj N, Yan KK, Gerstein MB (2010) Analysis of diverse regulatory networks in a hierarchical context shows consistent tendencies for collaboration in the middle levels. *Proc Natl Acad Sci U S A* 107:6841–6846.
22. Cancho RF, Janssen C, Solé RV (2001) Topology of technology graphs: small world patterns in electronic circuits. *Phys Rev E Stat Nonlin Soft Matter Phys* 64:046119.
23. Cancho RFI, Solé RV (2001) The small world of human language. *Proc Biol Sci* 268:2261–2265.
24. Valverde S, Sole RV (2005) Logarithmic growth dynamics in software networks. *Europhysics Letters* 72:858–864.
25. Adamic LA, Glance N (2005) The political blogosphere and the 2004 US Election.
26. Krackhardt D (1999) The ties that torture: Simmelian tie analysis in organizations. *Research in the Sociology of Organizations* 16:183–210.
27. Hanhijärvi S, Garriga GC, Puolamäki K (2009) Randomization Techniques for Graphs pp 780–791.
28. Marin J, Solé RV (1999) Macroevolutionary algorithms: a new optimization method on fitness landscapes. *IEEE Transactions on Evolutionary Computation* 3(4):272–286.